The Pennsylvania State University

The Graduate School

College of Earth and Mineral Sciences

MULTI-WELL ANALYTICAL SOLUTION FOR CONING UNDER SIMULTANEOUS STEADY-STATE FLOW OF THREE PHASES

A Thesis in

Energy and Mineral Engineering

by

Eunnam Ahn

Submitted in Partial Fulfillment
of the Requirements
for the Degree of

Master of Science

August 2018

The thesis of Eunnam Ahn was reviewed and approved* by the following:

Russell T. Johns

Professor of Petroleum and Natural Gas Engineering

Thesis Advisor

Gregory R. King

Professor of Practice, Petroleum and Natural Gas Engineering

Hamid Emami-Meybodi

Assistant Professor of Petroleum and Natural Gas Engineering

Luis F. Ayala H.

Professor and Associate Head

William A. Fustos Family Professor, Petroleum and Natural Gas Engineering

*Signatures are on file in the Graduate School.

ABSTRACT

A large amount of unwanted water and gas production from upward or downward coning can significantly erode profits in oil recovery processes. Simulation estimates of the magnitude and timing of coning can be erroneous owing to unknown reservoir heterogeneity, large grid blocks near the wells, and inaccuracies in simulation well models, such as that from Peaceman. This may lead to a failure to accurately calculate the critical oil rate in a given case. Thus, a good understanding of coning behavior is required for an effective water and gas control. An improved analytical water and gas control solution helps facilitate the computation of the critical rate and avoidance of unwanted water and gas. The solution may lead to a significant reduction in operating cost during oil production.

This thesis presents a multi-well steady-state analytical solution for coning of three phases (water, oil, and gas) flowing simultaneously. The solution for multiple wells is developed using the principle of superposition with a potential function that includes capillary pressure and relative permeability. The assumption of vertical equilibrium (VE) is made, which gives maximum vertical crossflow and therefore the largest possible coning. Any model for relative permeability and capillary pressure can be used, although we used Stone 2 for relative permeability and Brooks-Corey for capillary pressure. We give dimensionless inflow performance windows (IPW) to show the allowable physical window of three-phase rates and the maximum oil rate as a function of the water and the total well flow rate. The new potential functions are also used to demonstrate superposition for several well patterns with no-flow boundaries. Besides estimating critical oil rates, the

solution could be important to benchmark numerical solutions and improve the accuracy of Peaceman's well model.

TABLE OF CONTENTS

LIST OF FIGURES

NOMENCLATURE

Roman symbols

C	constant
g	gravity acceleration, m/s^2
h	total thickness of reservoir, m
k	permeability, m^2
k_r	relative permeability, *dimensionless*
L	hydraulic radius of influence, m
M	mobility ratio, *dimensionless*
N_b	bond number, *dimensionless*
N_G	gravity number, *dimensionless*
n_1	water relative permeability exponent, *dimensionless*
n_3	gas relative permeability exponent, *dimensionless*
n_{21}	oil relative permeability exponent in water-oil system, *dimensionless*
n_{23}	oil relative permeability exponent in oil-gas system, *dimensionless*
p	pressure, Pa
p_c	capillary pressure, Pa
p_d	capillary entry pressure, Pa
q	Darcy volumetric flow rate, m^3/s
R_L	effective aspect ratio, *dimensionless*

S normalized saturation, *dimensionless*

S_{jr} residual saturation of phase j, *dimensionless*

T transmissibility, $m^3/(Pa \cdot s)$

u Darcy volumetric flux, m/s

x linear distance along the x-axis, m

y linear distance along the y-axis, m

z elevation from the bottom of the reservoir, m

Greek letters

λ_j mobility of phase j, $m^2/(Pa \cdot s)$

λ_{rj} relative mobility of phase j, $1/(Pa \cdot s)$

μ viscosity, $Pa \cdot s$

ρ density, kg/m^3

Φ potential function, m^3/s

φ flow potential, Pa

Subscripts

D dimensionless variable

e location at the hydraulic radius of influence

i well index

j phase (w: water, o: oil, g: gas, l: liquid)

r radial direction

w location at wellbore

Superscripts

og oil-gas system

wo water-oil system

$\circ$ endpoint value

ACKNOWLEDGEMENTS

First and foremost, praises and thanks to the Almighty God, for his unconditional love throughout my studies. Without his blessings, this achievement would not have been possible.

I would like to express my sincere gratitude to my academic advisor, Dr. Russell T. Johns, for his continuous support, academic insights, patience, motivation and enthusiasm as well. It was indeed my privilege being his student and completing my degree under his advising.

Second, I would like to extend my gratitude to my committee members, Dr. Gregory R. King and Dr. Hamid Emami-Meybodi, for their helpful comments and suggestions on my research.

Next, I am extremely grateful to my family: my grandparents, my father, my mother and my brother, for their love, prayers and sacrifices for supporting me throughout my life.

Last, I would also like to show acknowledge my colleagues for their technical discussions and review of my thesis: Daulet Magzymov, Zhenke Xi and Prakash Purswani. This work would not have been possible without their help and support.

Chapter 1

INTRODUCTION

1.1 Description of the Problem

A large of amount of unwanted water or gas production from upward or downward coning can significantly erode profits in oil recovery processes. Simulation estimates of the magnitude and timing of coning can be erroneous owing to unknown reservoir heterogeneity, large grid blocks near the wells, and inaccuracies in simulation well models, such as that from Peaceman. Especially, the use of coarsely-gridded reservoir and/or Peaceman's well model can result in a significant error in estimates of coning and critical rates. Ideally, finely-gridded reservoir would be the solution to precisely capture the coning behavior, however, in that case, computational cost becomes an issue. Thus, it is necessary to keep a balance between the accuracy and the computational cost.

Coning behavior is a concern in the petroleum industry and thus there have been many studies to precisely describe the coning behavior near the wellbore region with an analytical solution. Recently, there have been several notable papers that have presented analytical solutions in a dimensionless "Dupuit form." Existing analytical coning solutions in a "Dupuit form" include simultaneous two-phase flow for any number of wells with Vertical Equilibrium (VE) and steady-state assumed. There has been an attempt to extend the solution to simultaneous three-phase flow, but only for a single well case without considering capillary pressure. Hence, analytical solutions for coning under simultaneous steady-state flow of three phases for any number of wells is desired.

1.2 Research Objectives

In this thesis, we extend the existing steady-state analytical solution for coning of three phases (water, oil, and gas) flowing simultaneously with any number of wells. The solution for multiple wells is developed using the principle of superposition with a potential function where arbitrary capillary pressure and relative permeability models can be included. Any model for relative permeability and capillary pressure can be used, although here we used Stone 2 for relative permeability and Brooks-Corey for capillary pressure. The assumption of vertical equilibrium (VE) is made, which gives the maximum vertical crossflow and therefore the largest possible coning. Based on the assumptions, the model becomes simple and intuitive: it will help both to precisely describe the coning behavior and considerably reduce the computational cost. The research objectives of the thesis are as follows:

1. to extend the existing analytical coning solutions for multiple wells from simultaneous flow of two phases to three phases. Furthermore, the solution should allow arbitrary capillary pressure and relative permeability models.
2. to investigate the sensitivity of key parameters that impact coning behavior.
3. to develop dimensionless inflow performance windows (IPW) that show the allowable physical window of three-phase rates and the maximum oil rate as a function of the water and the total well flow rate.

4. to allow the solution to be independent of the grid block size so that it can benchmark numerical solutions and potentially improve the accuracy of Peaceman's well model.

1.3 Outline of the Thesis

The thesis consists of five chapters and the organization is as follows: Chapter 2 first gives the literature review on the thesis. The methodology of the analytical coning solution is introduced in Chapter 3. Chapter 4 shows the results for the single well case and Chapter 5 shows the results for the multiple well cases. Last, summary and conclusions of the thesis are drawn with the achievements given in Chapter 6. Recommendations for future research is suggested in Chapter 6 as well.

Chapter 2

LITERATURE REVIEW

This chapter provides a background on the literature review related to the topic of this thesis: 1) Error near-wellbore, 2) Vertical Equilibrium (VE), and 3) Analytical coning solutions.

2.1 Errors Near-Wellbore

The use of a coarsely-gridded reservoir and/or Peaceman's well model (1978, 1983) can result in significant error in estimates of coning and critical rates. In large-scale reservoir simulation, grid blocks are not finely-gridded, thus it is unlikely to accurately capture subsurface phenomenon such as coning (Killough and Foster Jr., 1975). Furthermore, Peaceman (1978) developed a mathematical relationship between wellbore pressure and well block pressure in a two-dimensional uniform rectangular grid in homogeneous media with either isotropic or anisotropic permeability. Due to its simplicity, Peaceman's equation has been widely used in reservoir simulation. However, there are some limitations in the model itself which leads to an error while predicting subsurface behavior. There have been several studies that showed errors resulting from a coarsely-gridded reservoir and using Peaceman's well model (Sharma et al., 2011; Leeftink et al., 2015; Siripatrachai, 2016).

Sharma et al. (2011) showed that the grid block size affects several properties such as shear rate and injection rate while injecting polymer. Authors then stated that numerical simulation of polymer injection rates using Peaceman's well model and large grid blocks are not accurate since they cannot capture the effect of high velocity close to injection wells and numerical dispersion.

Leeftink et. al (2015) highlighted the importance of grid resolution near-wellbore by showing a significant error of gas injectivity near-wellbore while injecting gas in a Surfactant Alternating Gas (SAG) process. Authors found that poor grid resolution near-wellbore leads to a massive underestimation of the effect of dry-out, which increases injectivity in a SAG process and suggests the importance of finely-gridded blocks near the wellbore region. Furthermore, authors also pointed out that Peaceman equation (1978) assumes both uniform saturation and Newtonian mobility in the well grid block, which leads to erroneous results while injecting foam in a SAG process. Poor grid resolution near the well in numerical simulation leads to less increase in mobility near-wellbore, while the analytical solution presented by Leeftink et al. (2015) is able to model large mobility increases.

Siripatrachai (2016) showed the effect of the variation of grid block sizes near-wellbore. Results show that finely-gridded blocks near the wellbore region captures water saturation and water phase pressure better than coarsely-gridded blocks do, however at the same time requires additional computational cost.

Peaceman's model is still widely used today owing to its simplicity and is often the only option available in many commercial codes (IMEX, 2017; ECLIPSE, 2014). Sharpe and Ramesh (1992) modified Peaceman's well model to improve modeling of coning, however, their assumptions were too restrictive and unphysical since they assumed no gravity.

Ideally, a finely-gridded reservoir would be the best way to precisely capture the subsurface. However, in that case, computational cost becomes an issue. Thus, at some point, it is necessary to keep a balance between precision and computational cost. For this reason, in this thesis we present an analytical solution, which is unrelated to grid block size.

2.2 Vertical Equilibrium (VE)

Vertical equilibrium (VE) is a condition where all driving forces in the vertical direction sum to zero, resulting in hydrostatics (capillary-gravity equilibrium) as shown by Zapata and Lake (1981) and Lake et al. (2014). VE is often mistakenly thought to occur when flow is zero in the vertical direction. VE, however, implies immediate, infinite instantaneous flow in the vertical direction, and therefore gives maximum crossflow of fluids.

Coats et al. (1971) suggest that VE can be easily understood by an analogy with heat conduction. Consider there is a metal sheet with several feet in length but only quarter inch in thickness. In this case, two-dimensional heat conduction simulation can be implemented rather than three-dimensional in terms of thermal equilibrium because of its small thickness compared to its areal length.

Coats et al. (1967) validated the applicability of the VE assumption when there is a good vertical communication in a two-phase flow system by comparing two-dimensional areal simulation with a three-dimensional numerical simulation. Based on these results, the authors recommend the use of VE (when applicable) to reduce the computational cost by an order of magnitude.

Martin (1968) also validated VE and extended the previous work by Coats et al. (1967) into three-phase flow. In these two studies, in order to simplify the reservoir simulation into two-dimensional areal simulation, authors have implemented pseudo functions: pseudo relative permeability and pseudo capillary pressure.

Jacks et al. (1973) point out that pseudo functions cannot account for cases where flow rates drastically change and hence suggests using a dynamic pseudo function. By comparison to previous numerical verifications of VE concept, Yortsos (1995) theoretically proved the validity of VE with different conditions using an asymptotic analysis.

Lake et al. (2014) has shown the validity of the VE assumption. Assuming steady-state flow in a two-dimension Cartesian coordinates, the mass conservation equation for phase j is written as:

$$\frac{\partial}{\partial x_D}\left(\lambda_{rj}\frac{\partial \varphi_j}{\partial x_D}\right) + R_L^2\frac{\partial}{\partial z_D}\left(\lambda_{rj}\frac{\partial \varphi_j}{\partial z_D}\right) = 0, \tag{1}$$

where, R_L is a dimensionless scaling group called effective aspect ratio which is defined by:

$$R_L = \frac{L}{h}\sqrt{\frac{k_z}{k_x}}. \tag{2}$$

R_L can be understood as a ratio of characteristic time for fluid to move in the horizontal direction to that in the vertical direction (Lake et al., 2015). Thus, large R_L means that it takes relatively short time to move in the vertical direction. That is, large R_L corresponds to very good communication in the vertical direction, while small R_L to little communication in the vertical direction. Coning is less likely to occur for small R_L. Large R_L occurs in cases with:

1) large hydraulic radius of influence (L);
2) small reservoir thickness (h);
3) large vertical permeability (k_z); and,
4) small horizontal permeability (k_x).

Figure 2.1 shows the schematic reservoir and the concept of R_L. When R_L is large, fluids quickly equilibrate in the vertical direction compared to that in the horizontal direction (Lake et al., 2014; Coats et al., 1971). Hence, the equation can be decoupled into two parts:

$$\frac{\partial}{\partial x_D}\left(\lambda_{rj}\frac{\partial \varphi_j}{\partial x_D}\right) = 0, \tag{3}$$

$$R_L^2\frac{\partial}{\partial z_D}\left(\lambda_{rj}\frac{\partial \varphi_j}{\partial z_D}\right) = 0. \tag{4}$$

When VE (infinite R_L) is assumed and $\lambda_{r1} \neq 0$, the second equation implies that the vertical potential gradient of phase j is hydrostatic. With capillary and gravity forces present, we assume the potential is always in capillary-gravity equilibrium. VE assumption is generally satisfied when R_L is greater than about 10 (Zapata and Lake, 1981).

One of the advantages of making the VE assumption is that it reduces the dimension of the model by one (Coats et al., 1967; Martin, 1968; Jacks et al., 1973; Yortsos, 1995), which can save considerable computational time and allow for development of more complex analytical solutions.

The VE concept is widely used in petroleum engineering, groundwater contamination and also in CO_2 sequestration. In petroleum engineering, the "Dupuit form" of the analytical coning solution under VE has been developed through several studies (Delliste, 1998; Charbeneau et al., 2000; Obigbesan et al., 2001; David and Anim-addo, 2004; Johns et al., 2005; Ansari, 2006; Ansari and Johns, 2013; Phaiboonpalayoi and Johns, 2016). Details of some of these solutions will be introduced in the next section.

2.3 Analytical Coning Solutions

There have been many coning papers, which can be grouped into three categories: Analytical, numerical and empirical approach. Alikhan and Ali (1985) stated that analytical solutions provide an estimation of critical oil rate, which refers to a maximum oil rate that can be produced without any water or gas production. At the same time, authors pointed out that existing analytical approaches are limited in that they have certain restrictions like steady-state flow. However, analytical solutions are still useful because they provide simple computation of critical rate and not dependent on the grid block size (Ansari and Johns, 2013). In addition, the solutions can be used as a benchmark for numerical simulation (Ansari and Johns, 2013). Coning studies have mainly focused on estimating critical rate, water breakthrough time and water cut after breakthrough (Kuo and DesBrisay, 1983). In this thesis, we will focus on determination of the critical oil rate.

Dupuit (1863) assumed VE and steady-state between air and water in shallow wells. The Dupuit equation, however, assumes that only one-phase is being pumped and neglects capillary pressure and relative permeability.

Muskat and Wyckoff (1935) derived an approximate steady-state solution for two-dimensional water coning in an oil reservoir. Authors assumed single phase flow in the development of the solution. That is, oil is in steady-state flow, water is static and not produced. Numerous other authors have subsequently examined analytical steady-state coning solutions for a vertical well (Arthur, 1944; Meyer and Garder, 1954; Chaney et al., 1956; Chierici et al., 1964; Chappelear and Hirasaki, 1976; Pirson, 1977; Wheatley, 1985; Piper and Chaperon, 1986; Piper and Gonzalez Jr., 1987; Abass and Bass, 1988; Høyland et al., 1989; Guo and Lee, 1993; Pietraru and Le Bars, 1996; Gunning et al., 1999; Armenta and Wojtanowicz, 2002; Siemek and Stopa, 2002; Utama, 2008; Tabatabaei et al., 2012).

Arthur (1944) extended the work of Muskat and Wyckoff (1935) into simultaneous water and gas coning to dipping and layered beds and presented a trial and error solution for simultaneous gas and water coning. Authors also developed charts to solve gas and water coning behavior based on Muskat's solution. Results show that the distance of the well from the static interface of the two fluids is critical, with coning occurring even for small drawdowns.

Meyer and Garder (1954) presented an analytical solution for critical oil rate in a three-phase reservoir in a homogeneous formation. Authors assumed radial flow and that only one phase flows while the other two phases are static.

Chaney et al. (1956) studied three-phase coning based on a potentiometric model and mathematical analysis. Authors included completions at any depth in a homogeneous and isotropic reservoir.

Starting from the water and gas coning theory of Muskat and Wyckoff (1935), Chierici et al. (1964) developed a set of curves using electrical analogy for two types of problems: 1) Critical oil rate when reservoir and fluid properties are only given and 2) critical oil rate when reservoir properties, fluid properties and the length and position of perforated interval are given. Authors assumed that the formation is homogeneous, the underlying aquifer is very small, and the gas cap expands at a very small rate.

Chappelear and Hirasaki (1976) derived an analytical coning solution using the VE assumption and segregated flow. Authors also assumed radially symmetric, homogeneous, anisotropic reservoir with a partially perforated well. Fluids are assumed to be incompressible.

Pirson (1977) extended Dupuit's segregated flow solution to account for a third phase (oil), two of which are static (water and gas). Authors presented a case where oil is produced from a thin oil column underlaid by bottom water and overlain by gas. Based on this condition, determination of critical rate was shown with a relation between the depth of the well penetration into the pay thickness and the completion interval. That is, Pirson's solution has been used to estimate the maximum oil rate to avoid upward coning of water and downward coning of gas into the perforated well.

Wheatley (1985) developed a two-phase flow analytical solution for critical rate where oil flows into a partially penetrating well underlain by water. Fluids are assumed to be incompressible.

Piper and Chaperon (1986) provided equations to estimate critical rate in horizontal wells in an anisotropic formation. The critical rate in a vertical well in an anisotropic formation - including the influence of distance between well and boundary - is also derived. Coning is more sensitive to anisotropy: critical rate slightly increases while vertical permeability decreases, but the critical cone elevation does not change significantly. It is observed that critical cones become closer to horizontal wells than to vertical wells. That is, critical rate is higher in horizontal wells than in vertical wells, but this advantage lessens when anisotropy increases. Thus, the critical rate in a horizontal well needs to be estimated carefully from key parameters.

Piper and Gonzalez Jr. (1987) presented a calculation method for critical rate and optimum completion interval in an oil reservoir overlain by a gas cap and underlain by an aquifer. Authors extended the solution of Wheatley (1985), where fluid potential and critical rate for two-phase flow have been calculated, into three-phase flow. Authors also showed that previous studies, which neglected the effect of cone rise on fluid potential, failed to precisely calculate the critical rate.

Abass and Bass (1988) developed an analytical solution for water coning under different conditions. Authors calculated the critical rate for steady-state and pseudo steady-state flow in a two-dimensional radial flow system using an averaged pressure concept.

Hoyland et al. (1989) presented practical correlations to predict critical rate for water coning based on a large number of simulation runs with a general numerical reservoir model. Results are limited to a well perforated from the top of the formation.

Gunning et al. (1999) proposed an analytical coning solution for dual completion in order to mitigate water coning in thin oil column reservoirs. The solution has been compared with a numerical simulation. In addition, authors presented a dimensionless inflow performance window (IPW), which they call "safety-zones" to show the physical region where water-free oil can be produced. Furthermore, authors also showed the effect of heterogeneity to coning.

More recently the analytical approach of Dupuit has been extended to provide more realistic coning solutions (Delliste, 1998; Charbeneau et al., 2000; Obigbesan et al., 2001; Johns et al., 2005; Ansari, 2006; Ansari and Johns, 2013; Phaiboonpalayoi and Johns, 2016). Delliste (1998) developed a new dimensionless analytical coning solution in a "Dupuit form" for simultaneous steady-state flow of two phases from a single vertical well, including capillary pressure and relative permeability. Authors has also showed a steady-state coning solution for three-phase flow using the Brooks-Corey-Burdine (BCB) model, however it was not for simultaneous three-phase flow. They allowed only one phase or two phases to be produced simultaneously. Furthermore, there was a slight error in the derivation of averaged relative permeability for oil phase using the BCB model in a dimensionless form. In addition, for simplicity, author used a simple k_{ro} model, which is suggested by Charbeneau and Chiang (1995). The author has only shown a limiting case where capillary pressure is neglected. Furthermore, author developed the first dimensionless inflow performance windows (IPW) for physical operating rates, where the critical oil rates are given. Author then showed how the window changes after varying several parameters, respectively. In addition, the author showed that the oil rate could be substantially increased by increasing the water flow rate and applied this notion to skimmer pumps in aquifer remediation. The technology has also been applied to Downhole Water-Sink (DWS) technology (Swisher and Wojtanowicz, 1995; Swisher and Wojtanowicz, 1996; Shirman and Wojtanowicz, 2000) for the oil field.

Strack (1989) developed a potential function for several cases including a freshwater pumping well located near a coastal aquifer and used this function to develop a multi-well solution using the principle of superposition. Obigbesan et al. (2001) developed an analytical solution that estimates the maximum rate of LNAPL for skimmer-, single-, dual pump wells. Succeeding the work of Obigbesan et al. (2001), David and Anim-Addo (2004) extended the existing analytical coning solution from a single well to multiple wells. For the multi-well solution, David and Anim-Addo (2004) superposed the single well solution using a potential function.

Ansari and Johns (2013) then expanded the existing dimensionless analytical coning solution for a single well to allow for multiple wells using superposition of their derived potential function. The effect of capillary pressure and relative permeability were included in the potential function. Authors validated their analytical solution against finely-gridded reservoir simulation. Comparison shows that when they increased the effective aspect ratio (R_L), the result approached the analytical solution, which assumed VE.

Phaiboonpalayoi and Johns (2016) presented a single well coning solution for simultaneously steady flow of three phases (water, oil, and gas), but did not allow for capillary pressure or relative permeability in their solution or for multiple wells. Authors partially introduced the Stone 2 model in a dimensionless form, however, did not include it into their solution. In addition, authors have not showed the multiple well case for vertical wells. That is, they have just shown the three-phase analytical coning solution assuming constant permeability in a single-well without capillary pressure.

In summary, many dimensionless “Dupuit form” of coning solutions for simultaneous steady-state flow for two phases have been published. Earlier, both single-well and multi-well cases have been shown for two-phase flow. For BCB model, the derivation of BCB model for averaged relative permeability has been introduced and implemented, however without simultaneous three-phase flow (only one-phase or simultaneous flow of two phases). For the Stone 2 model, the derivation was partially introduced but was not included into the solution. Additionally, only the single-well case has been shown. In this thesis, we show the solution using Stone 2 model for averaged relative permeability. Furthermore, we extend the single-well solution into a multiple well solution.

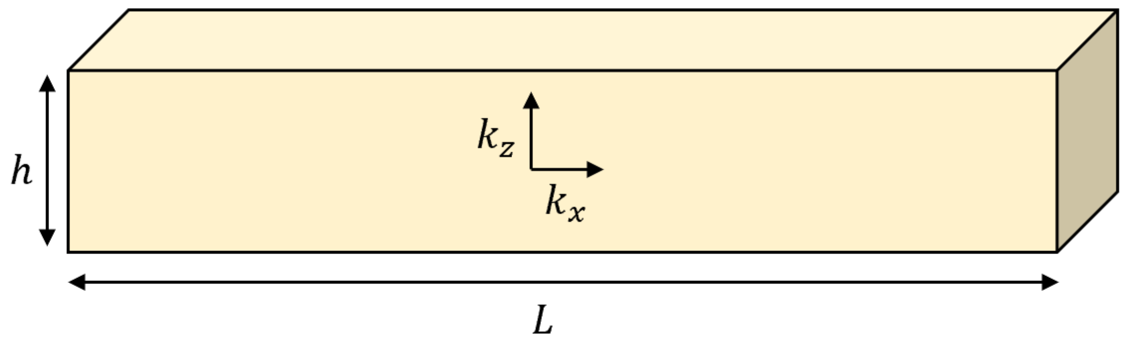

Figure 2.1 Schematic of the reservoir to show the concept of R_L

Chapter 3

METHODOLOGY

We assume three-phase immiscible flow (water, oil, and gas) as shown in Figure 3.1, with assumptions similar to those made in previous papers (Delliste, 1998; Charbeneau et al., 2000; Obigbesan et al., 2001; David and Anim-addo, 2004; Johns et al., 2005; Ansari, 2006; Ansari and Johns, 2013; Phaiboonpalayoi and Johns, 2016). That is,

1) there are at most three phases and all fluids are immiscible and incompressible;
2) fluids flow radially towards the vertical wellbore of radius, r_w, at a constant volumetric flow rate, q_t, where $q_t = q_w + q_o + q_g$;
3) fluids are in steady-state and in vertical equilibrium (VE), which leads to maximum crossflow of fluids in the vertical direction (details of the VE assumption can be found in Chapter 2);
4) fluid viscosities and densities are constant;
5) ρ_w is assumed greater than ρ_o and ρ_o greater than ρ_g;
6) flow is isothermal;
7) the thickness of the reservoir is constant, h;
8) the reservoir is homogeneous and isotropic;
9) the thickness of each phase is as follows: h_w is from the bottom of the reservoir to the level where $p_c^{wo} = 0$, h_o is from the level where $p_c^{wo} = 0$ to the level where $p_c^{og} = 0$, and h_g is from the level where $p_c^{og} = 0$ to the top of the reservoir; and,

10) at distance r_e, the thickness of each phase is constant and equal to h_{we}, h_{oe} and h_{ge}, respectively.

When capillary pressure is neglected (the Bond numbers N_b^{wo} and N_b^{og} are infinite), the elevation at which $p_c^{wo} = 0$ is the same as the water-oil contact (WOC), and the $p_c^{og} = 0$ level corresponds to the gas-oil contact (GOC). Otherwise, the $p_c^{og} = 0$ level is always below the GOC and $p_c^{wo} = 0$ is always below the elevation of the WOC. Details are shown in Figure 3.1. The fluid levels in Figure 3.1 are illustrative only and can change significantly depending on the flow rates and the initial thickness of each phase.

3.1 Single Well Solution for Simultaneous Three-Phase Flow

The radial mass balance equation for phase j integrated from the bottom to the top of the reservoir is:

$$\int_0^h \left[\frac{1}{h}\frac{d}{dr}\left(ru_j\right)\right] dz = 0, \tag{1}$$

where, u_j is the horizontal Darcy's flux of phase j given by $u_j = -\lambda_j \frac{d\varphi_j}{dr}$. The parameter λ_j is the mobility of phase j and φ_j is the flow potential of phase j. Substitution of Darcy's flow equation into Eq. (1) yields:

$$\frac{1}{r}\frac{d}{dr}\left[r\bar{\lambda}_j h \frac{d\varphi_j}{dr}\right] = 0, \tag{2}$$

where, $\bar{\lambda}_j$ is defined as $\bar{\lambda}_j = \frac{1}{h}\int_0^h \lambda_j \, dz = \lambda_j^{\circ} \bar{k}_{rj}$, and $\lambda_j^{\circ} = \frac{k k_{rj}^{\circ}}{\mu_j}$. The potential function for each phase, Φ_j, is given by $\frac{d\Phi_j}{dr} = T_j \frac{d\varphi_j}{dr}$, where, T_j is the transmissibility of phase j, defined as $T_j = \int_0^h \lambda_j \, dz = \bar{\lambda}_j h$. Integration of the potential function yields:

$$\Phi_j = \int \left(T_j \frac{d\varphi_j}{dr} \right) dr + C, \tag{3}$$

where the integration constant is arbitrary. The transmissibility accounts for any relative permeability and capillary pressure model. Using the potential function, Eq. (2) becomes the Laplace equation:

$$\frac{1}{r}\frac{d}{dr}\left[r \frac{d\Phi_j}{dr} \right] = 0; \quad \nabla^2 \Phi_j = 0. \tag{4}$$

The general solution to the Laplace equation for a single well producing at a constant volumetric rate q_j is:

$$\Phi_j = \frac{q_j}{2\pi} \ln r + C. \tag{5}$$

For a single well, the constant C is determined from a known value within the reservoir, typically at a large radial distance from the well where $h_j = h_{je}$ at $r_j = r_{je}$ so that Eq. (5) becomes $\Phi_j - \Phi_{je} = \frac{q_j}{2\pi} \ln \frac{r}{r_e}$. Thus, the potential function can be easily determined as a function of radial distance, r.

The potential function is also a complicated expression of the phase levels. Appendix A derives the thickness of each phase with distance, which when substituted into Eq. (3) gives the potential function in terms of the thickness of phase j. For simultaneous three-phase flow, the potential functions for each phase are:

$$\Phi_w = \frac{q_w}{2\pi}\int_{h_w}^{h_{we}} \frac{dh_w}{\frac{1}{\Delta\rho_{wo}g}\left(\frac{q_w}{2\pi T_w} - \frac{q_o}{2\pi T_o}\right)} + \Phi_{we}, \tag{6}$$

$$\Phi_o = \frac{q_o}{2\pi}\int_{h_o}^{h_{oe}} \frac{dh_o}{\left(\frac{1}{\Delta\rho_{wo}g} + \frac{1}{\Delta\rho_{wo}g}\right)\frac{q_o}{2\pi T_o} - \frac{1}{\Delta\rho_{og}g}\frac{q_g}{2\pi T_g} - \frac{1}{\Delta\rho_{wo}g}\frac{q_w}{2\pi T_w}} + \Phi_{oe}, \tag{7}$$

$$\Phi_g = \frac{q_g}{2\pi}\int_{h_g}^{h_{ge}} \frac{dh_g}{\frac{1}{\Delta\rho_{og}g}\left(\frac{q_g}{2\pi T_g} - \frac{q_o}{2\pi T_o}\right)} + \Phi_{ge}. \tag{8}$$

The integrals in Eqs. (6) to (8) can be computed to specified accuracy using numerical integration with any relative permeability or capillary pressure model, although the Stone 2 relative permeability model (1973) and Brooks-Corey capillary pressure model (1964) are used in this thesis. For simplified models, Eqs. (6) to (8) can be solved exactly without numerical integration.

Dimensionless variables are widely used to improve scaling, avoid unit conversions and to generate type curves (Shook et al., 1992). Scaling groups used for a single well are:

1) dimensionless potential function: $\Phi_{Dj} = -\left(2\pi\Phi_j\right)/q_t$;
2) dimensionless radial distance: $r_D = r/r_w$ and $r_{De} = r_e/r_w$;
3) dimensionless thickness of phase j at radius r_{De}: $h_{Dj} = h_j/h$;

4) dimensionless flow rate for phase j: $q_{Dj} = q_j/q_t$;

5) gravity number: $N_b^{wo} = -(2\pi h^2 \lambda_o^\circ \Delta\rho_{wo} g)/q_t$ and $N_b^{og} = -\left(2\pi h^2 \lambda_o^\circ \Delta\rho_{og} g\right)/q_t$;

6) endpoint mobility ratio: $M_{wo}^\circ = \lambda_w^\circ/\lambda_o^\circ$ and $M_{og}^\circ = \lambda_g^\circ/\lambda_o^\circ$; and,

7) dimensionless density ratio: $\rho_{Do} = \rho_o/\rho_w$ and $\rho_{Dg} = \rho_g/\rho_w$.

The flow rate q_t is the total flow rate in well i, where $q_{Dw} + q_{Do} + q_{Dg} = 1$. Because of the choice of dimensionless groups, the total flow rate is specified, while two of the three phase flow rates can be independently specified. The minus sign is added in (1) and (5) to make the group values positive for production. This comes from the fact that all flow rates (q_t, q_w, q_o, and q_g) are negative for production. A subscript i is added to (1) and (5) when multiple wells are used with different total rates. For multiple wells, the total flow rate in (1) is based on one of the wells. The solution now becomes:

$$\ln\frac{r_D}{r_{De}} = N_G^{wo}\int_{h_{Dw}}^{h_{Dwe}} \frac{dh_{Dw}}{\frac{q_{Do}}{\bar{k}_{ro}} - \frac{1}{M_{wo}^\circ}\frac{q_{Dw}}{\bar{k}_{rw}}}, \tag{9}$$

$$\ln\frac{r_D}{r_{De}} = N_G^{wo}\int_{h_{Do}}^{h_{Doe}} \frac{dh_{Do}}{\left(\frac{1-\rho_{Do}}{\rho_{Do}-\rho_{Dg}}\right)\frac{1}{M_{og}^\circ}\frac{q_{Dg}}{\bar{k}_{rg}} + \frac{1}{M_{wo}^\circ}\frac{q_{Dw}}{\bar{k}_{rw}} - \left(\frac{1-\rho_{Dg}}{\rho_{Do}-\rho_{Dg}}\right)\frac{q_{Do}}{\bar{k}_{ro}}}, \tag{10}$$

$$\ln\frac{r_D}{r_{De}} = N_G^{og}\int_{h_{Dg}}^{h_{Dge}} \frac{dh_{Dg}}{\frac{q_{Do}}{\bar{k}_{ro}} - \frac{1}{M_{og}^\circ}\frac{q_{Dg}}{\bar{k}_{rg}}}. \tag{11}$$

3.2 Multiple Well Solution for Simultaneous Three-Phase Flow

The Laplace equation is a linear differential equation that satisfies the principle of superposition. Thus, the solution for the potential function for a multi-well system with N wells is:

$$\Phi_j = \sum_{i=1}^{N} \Phi_{ji} = \sum_{i=1}^{N} \frac{q_{ji}}{2\pi} \ln r_i + C. \tag{12}$$

The subscript i is the well index and C is a constant determined at any point in the reservoir where the thickness of each phase is known. The radial distance r_i from well i to any point in the reservoir is:

$$r_i = \sqrt{(x - x_i)^2 + (y - y_i)^2}. \tag{13}$$

Application of the outer boundary condition at known thickness of each phase (x_e, y_e) in the reservoir $\left(\Phi_j(x_e, y_e) = \Phi_{je}\right)$ gives:

$$\Phi_j = \sum_{i=1}^{N} \frac{q_{ji}}{2\pi} \ln \frac{r_i}{r_{ei}} + \Phi_{je}, \tag{14}$$

where, $r_{ei} = \sqrt{(x_e - x_i)^2 + (y_e - y_i)^2}$.

With the scaling groups, conversion of Eqs. (14) and (6) to (8) into a dimensionless form gives:

$$\Phi_{Dj} = \sum_{i=1}^{N} q_{Dji} \left(\frac{q_{ti}}{q_{t1}}\right) \ln \frac{r_{Di}}{r_{Dei}} + \Phi_{Dje}, \tag{15}$$

and

$$\Phi_{Dw} = \sum_{i=1}^{N} \Phi_{Dwi} = \sum_{i=1}^{N} q_{Dwi} N_{G1}^{wo} \int_{h_{Dw}}^{h_{Dwe}} \frac{dh_{Dw}}{\frac{q_{Doi}}{\bar{k}_{ro}} - \frac{q_{Dwi}}{M_{wo}^{\circ} \bar{k}_{rw}}} + \Phi_{Dwe}, \tag{16}$$

$$\begin{aligned} \Phi_{Do} &= \sum_{i=1}^{N} \Phi_{Doi} \\ &= \sum_{i=1}^{N} q_{Doi} N_{G1}^{wo} \int_{h_{Do}}^{h_{Doe}} \frac{dh_{Do}}{\left(\frac{1-\rho_{Do}}{\rho_{Do}-\rho_{Dg}}\right) \frac{q_{Dgi}}{M_{og}^{\circ} \bar{k}_{rg}} + \frac{q_{Dwi}}{M_{wo}^{\circ} \bar{k}_{rw}} - \left(\frac{1-\rho_{Dg}}{\rho_{Do}-\rho_{Dg}}\right) \frac{q_{Doi}}{\bar{k}_{ro}}} + \Phi_{Doe}, \end{aligned} \tag{17}$$

$$\Phi_{Dg} = \sum_{i=1}^{N} \Phi_{Dgi} = \sum_{i=1}^{N} q_{Dgi} N_{G1}^{og} \int_{h_{Dg}}^{h_{Dge}} \frac{dh_{Dg}}{\frac{q_{Doi}}{\bar{k}_{ro}} - \frac{q_{Dgi}}{M_{og}^{\circ} \bar{k}_{rg}}} + \Phi_{Dge}. \tag{18}$$

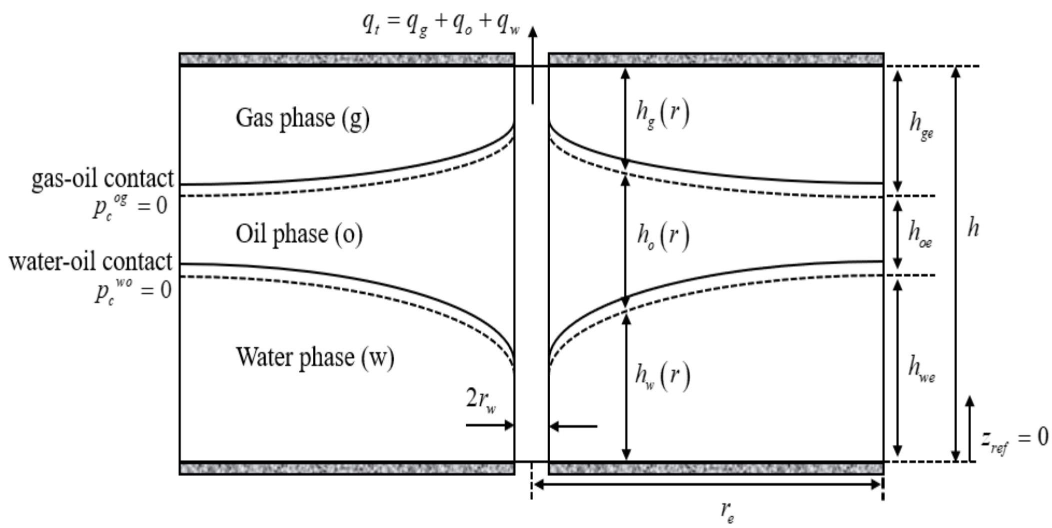

Figure 3.1 Schematic of the reservoir model for steady-state three-phase flow. Dashed lines are the elevations of zero capillary pressure, while solid lines correspond to drainage capillary entry pressures (contacts between two phases).

Chapter 4

RESULTS FOR SINGLE WELL CASE

Chapters 4 and 5 give example coning calculations for simultaneous flow of three phases. First, we show the phase thicknesses for a single well with one no-flow boundary (case 1) in Chapter 4, where solutions are constructed with and without capillary pressure to illustrate its effect on fluid levels. For the single well case we also give dimensionless inflow performance windows (IPW) to illustrate the boundaries of the possible physical rates with and without capillary pressure. The limit of these physical rates is a critical value, where a given phase flow rate cannot be exceeded.

The total flow rate is constant for each well, so that one of the phase flow rates is dependent on the two other rates. That is, we always have $q_{Dw} + q_{Do} + q_{Dg} = 1$, where in this paper the gas rate is generally the dependent flow rate. A change in the total flow rate impacts the dependent phase flow rate, and also the two gravity numbers.

4.1 Single well with infinite flow boundary (Case 1)

In this example, the dimensionless radial distance of the reservoir (r_{De}) to constant potential is taken to be 1,000. Because phase thicknesses change the most near a well, the radial distance is shown in log scale from $r_D = 1$ (at the wellbore) to $r_D = 25$ in all figures.

Figure 4.1 shows the fluid levels with and without capillary pressure, but for the case where the oil flow rate is critical. The water rate is constant for both solutions, while the gas rate changes as needed for a constant total rate. The critical oil rate is found where the dimensionless oil thickness (h_{Do}) at the wellbore becomes zero. The zero capillary pressure case corresponds to infinite Bond number, while the Bond numbers of $N_b^{wo} = 100$ and $N_b^{wo} = 50$ are used to represent nonzero capillary pressure. The results show that as capillary pressure is included, the critical oil rate decreases from 0.61 to 0.33, a factor of about 2.0. The smaller critical oil rate with capillary pressure results from a decreased oil thickness, which is partly the result of a larger entry height for oil-water than for gas-oil. The two critical oil rates in Figure 4.1 with and without capillary pressure are marked as point A and B in Figure 4.8, respectively, as is discussed later.

The dimensionless flow rate of each phase is varied in Figures 4.2 to 4.4. Capillary pressure is included ($N_b^{wo} = 100$ and $N_b^{wo} = 50$) in all three figures, and in each case the corresponding critical phase rate is shown. Figure 4.2 shows the thickness along the cross section of the reservoir as q_{Dw} is varied, while q_{Do} is fixed at 0.2. When q_{Dw} increases from 0 to 0.5, the gas cone slightly increases, while water cones more downward. The water-oil contact (WOC) is sensitive to the flow rate changes. These sensitivities are related to the assumption of VE and the contrast in densities between the fluids. As a denser phase is produced, the other phases react to that loss of mass so that VE (instantaneous hydrostatics) is restored.

Figure 4.3 shows the phase levels for changes in q_{Do} while q_{Dw} is fixed at 0.5. When q_{Do} increases from 0.2 to 0.4, the gas slightly cones down towards the oil phase, while water cones up towards the oil phase. The result shows a greater sensitivity to the WOC as the oil flow rate changes, than for the GOC. When q_{Do} is 0.4, the dimensionless oil thickness became zero, which is the maximum q_{Do} at the given condition (the critical oil rate for that case).

The gas flow rate q_{Dg} is varied in Figure 4.4 while q_{Dw} is fixed at 0.18 (thus the oil rate is the dependent rate here). When q_{Dg} increases from 0.6 to 0.8, gas coning increases upward, while the water cone moves significantly downward. This large change in the water level is because q_{Do} decreases as q_{Dg} increases. The total flow rate is again constant. The rate with $q_{Dg} = 0.8$ is the critical gas rate, because the gas thickness becomes zero then.

Figure 4.5 shows the sensitivity of bond number (N_b^{wo} and N_b^{og}) on the thickness of each phase along a cross-section of the reservoir. Three cases are shown: The black, red and blue lines show the case where ($N_b^{wo} = 100, N_b^{og} = 50$), ($N_b^{wo} = 500, N_b^{og} = 250$), and ($N_b^{wo}, N_b^{og}$= infinite). Results show that as bond number increases, gas cones up and water cones down. Small bond number results in the oil thickness to decrease at the same flow rates. That is, critical oil rate will decrease as bond number decreases under the given condition.

Figure 4.6 shows the sensitivity of oil density ratio (ρ_{Do}) on the thickness of each phase along a cross-section of the reservoir. Three cases are shown: The black, red, and blue line show the case where $\rho_{Do} = 0.7$, $\rho_{Do} = 0.8$, and $\rho_{Do} = 0.9$. Flow rates are $q_{Dw} = 0.3$, $q_{Do} = 0.5$, and $q_{Dg} = 0.2$ for all three cases. Result shows that critical oil rate decreases as ρ_{Do} increases.

Figure 4.7 shows the sensitivity of the gas density ratio (ρ_{Dg}) on the thickness of each phase along a cross-section of the reservoir. Three cases are shown: The black, red, and blue line show the case where $\rho_{Dg} = 0.1$, $\rho_{Dg} = 0.15$, and $\rho_{Dg} = 0.2$. Flow rates are $q_{Dw} = 0.3$, $q_{Do} = 0.5$, and $q_{Dg} = 0.2$ for all three cases. Result shows that gas density ratio does not affect the gas-oil contact (GOC) and water-oil contact (WOC) as much compared to that of the oil density ratio. Furthermore, critical oil rate decreases as ρ_{Dg} increases.

The inflow performance window (IPW) in Figure 4.8 demonstrates the physical boundaries of the flow rates that cannot be exceeded. The total flow rate is constant here, as opposed to the IPW plots presented by Delliste (1998) and Johns et al. (2005). First consider the red curves, which gives the physical region when capillary pressure is included ($N_b^{wo} = 100$ and $N_b^{wo} = 50$). The left upper boundary of the window is where the dimensionless water thickness equals zero, while the lower right boundary of the window corresponds to zero dimensionless oil thickness. The boundary at the lower left is where the dimensionless gas thickness zero. The dashed line is where $q_{Do} + q_{Dw} = 1$ and $q_{Dg} = 0$. The physical operating region is therefore within these limiting curves, and is shaded gray. The blue curves show the change in the physical operating region when capillary pressure is neglected (both N_b^{wo} and N_b^{wo} are infinite). For the blue curves, the boundary where the dimensionless gas thickness becomes zero does not exist. That is, the gas rate can equal the total well flow rate.

The physical region for the IPW curves with capillary pressure is narrower than the case where capillary pressure is zero. This means capillary pressure decreases the critical oil rates by about a factor of 2.0, for the parameters used. That is, the flow rates are more restricted when capillary pressure is included. For example, in Figure 4.8, the critical oil rate where capillary pressure is included is 0.33 (point A) while the critical oil rate where capillary pressure is neglected is 0.61 (point B).

IPWs can be changed by varying several parameters such as the density gas ratio (ρ_{Dg}), Bond numbers (N_b^{wo} and N_b^{og}), Gravity numbers (N_G^{wo} and N_G^{og}), and the initial thicknesses of the phases (h_{Dw}, h_{Do}, and h_{Dg}). In practice, the oil flow rate could be maximized by locating the perforations in such a way to minimize gas and water production. The oil flow rate could also be increased by independently increasing the gas and water rates using a complex wellbore completion similar to what is used in Downhole Water-Sink (DWS) technology.

Figures 4.9 and 4.10 show the change of the dimensionless IPWs where several parameters are varied. Figure 4.9 shows the dimensionless IPW where both Gravity numbers are increased compared to that of Figure 4.8. Result shows that the size of the physical region increased as both Gravity numbers increase. There are many factors that affect the Gravity numbers but if the increase resulted from the endpoint mobility of oil (λ_o°), it means mobility of the oil increased in this condition. That is, under this condition, oil is relatively easily movable, which results in the expansion of the physical operating region.

Figure 4.10 shows the dimensionless IPW where dimensionless oil thickness decreased from 0.55 to 0.3. Result shows that the physical region became narrower as dimensionless oil thickness decreases. That is, the decrease in the dimensionless oil thickness decreased at the boundary condition means that there is less oil that could be produced from the reservoir, which results in the physical region where oil can be produced.

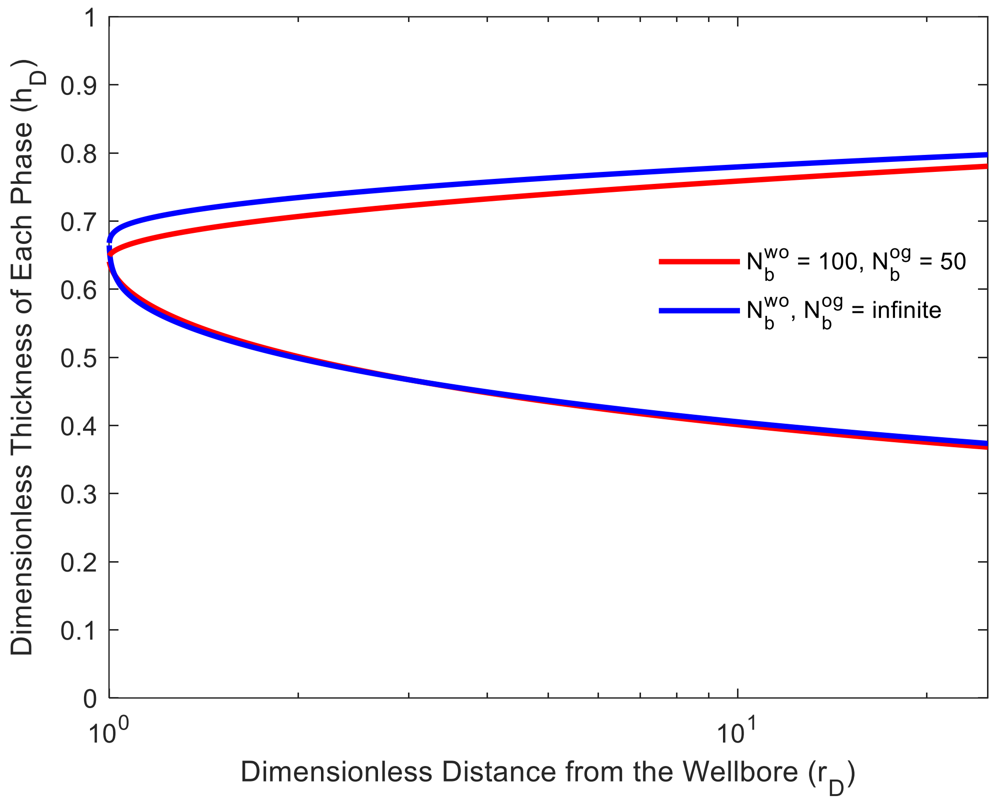

Figure 4.1 Dimensionless thickness of each phase along a cross-section of the reservoir at the critical oil rate with and without capillary pressure. The red line includes capillary pressure ($N_b^{wo} = 100$ and $N_b^{og} = 50$, $q_{Dw} = 0.3$, $q_{Do} = 0.33$, and $q_{Dg} = 0.37$), while the blue line is when capillary pressure is neglected (both N_b^{wo} and N_b^{og} are infinite, $q_{Dw} = 0.3$, $q_{Do} = 0.61$, and $q_{Dg} = 0.09$).

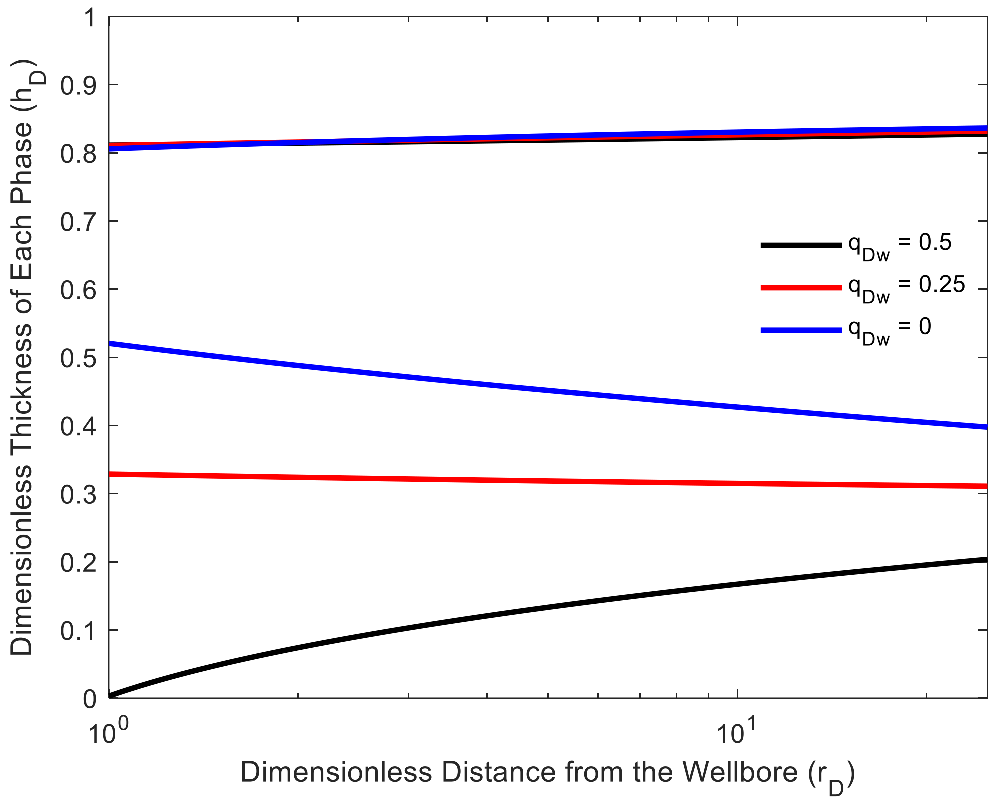

Figure 4.2 Dimensionless thickness of each phase along a cross-section of the reservoir while varying the dimensionless water flow rate, q_{Dw}. The black, red, and blue line show the case where ($q_{Dw} = 0$, $q_{Do} = 0.2$, and $q_{Dg} = 0.8$), ($q_{Dw} = 0.25$, $q_{Do} = 0.2$, and $q_{Dg} = 0.55$), and ($q_{Dw} = 0.5$, $q_{Do} = 0.2$, and $q_{Dg} = 0.3$), respectively. q_{Do} is fixed and capillary pressure is included ($N_b^{wo} = 100$ and $N_b^{og} = 50$) for all three cases.

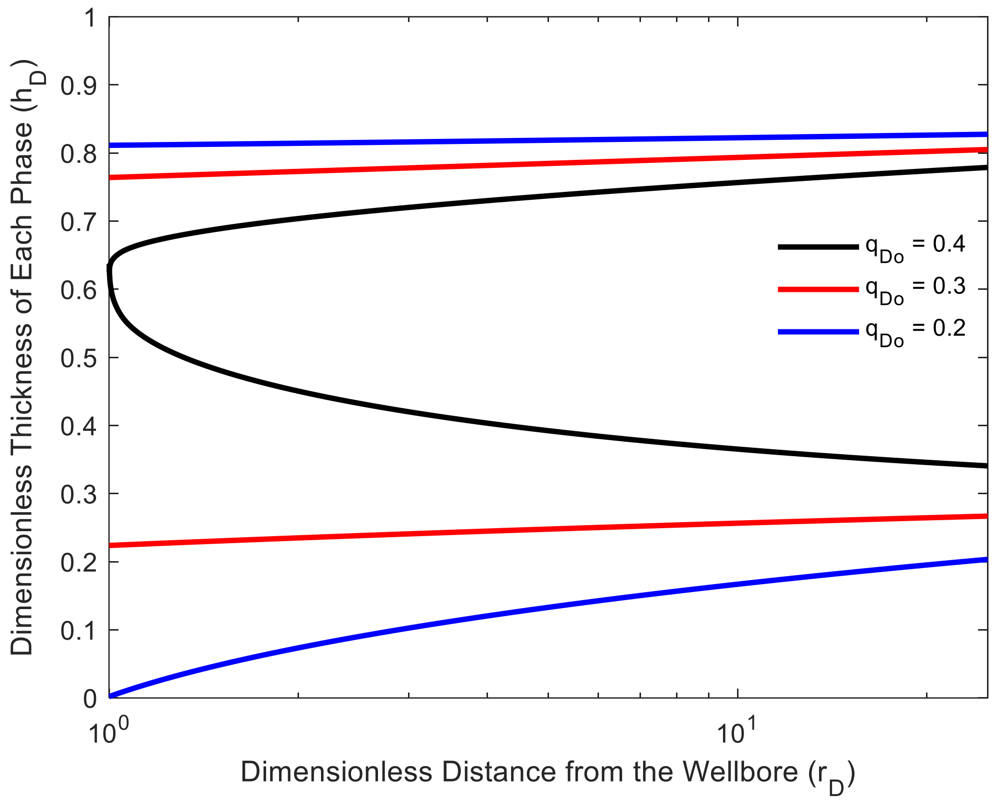

Figure 4.3 Dimensionless thickness of each phase along a cross-section of the reservoir while varying the dimensionless oil flow rate, q_{Do}. The black, red, and blue line show the case where ($q_{Dw} = 0.5$, $q_{Do} = 0.4$, and $q_{Dg} = 0.1$), ($q_{Dw} = 0.5$, $q_{Do} = 0.3$, and $q_{Dg} = 0.2$), and ($q_{Dw} = 0.5$, $q_{Do} = 0.2$, and $q_{Dg} = 0.3$), respectively. q_{Dw} is fixed and capillary pressure is included ($N_b^{wo} = 100$ and $N_b^{og} = 50$) for all three cases.

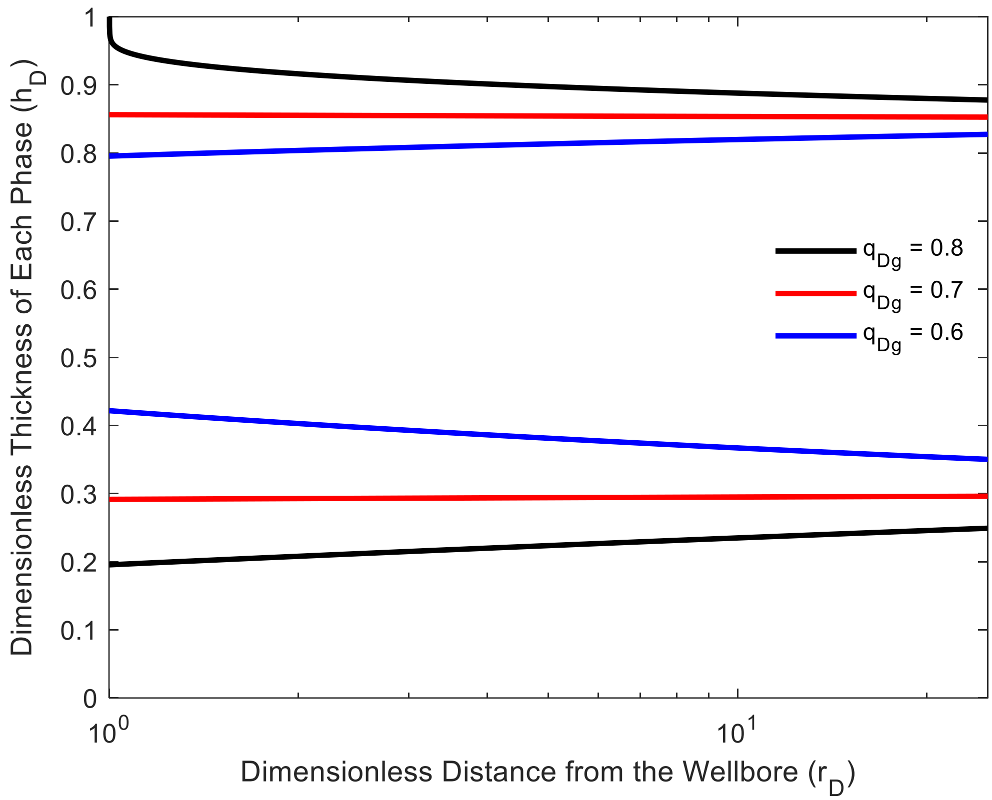

Figure 4.4 Dimensionless thickness of each phase along a cross-section of the reservoir while varying the dimensionless gas flow rate, q_{Dg}. The black, red, and blue line show the case where ($q_{Dw} = 0.18$, $q_{Do} = 0.022$, and $q_{Dg} = 0.8$), ($q_{Dw} = 0.18$, $q_{Do} = 0.12$, and $q_{Dg} = 0.7$), and ($q_{Dw} = 0.18$, $q_{Do} = 0.22$, and $q_{Dg} = 0.6$), respectively. q_{Dw} is fixed and capillary pressure is included ($N_b^{wo} = 100$ and $N_b^{og} = 50$) for all three cases.

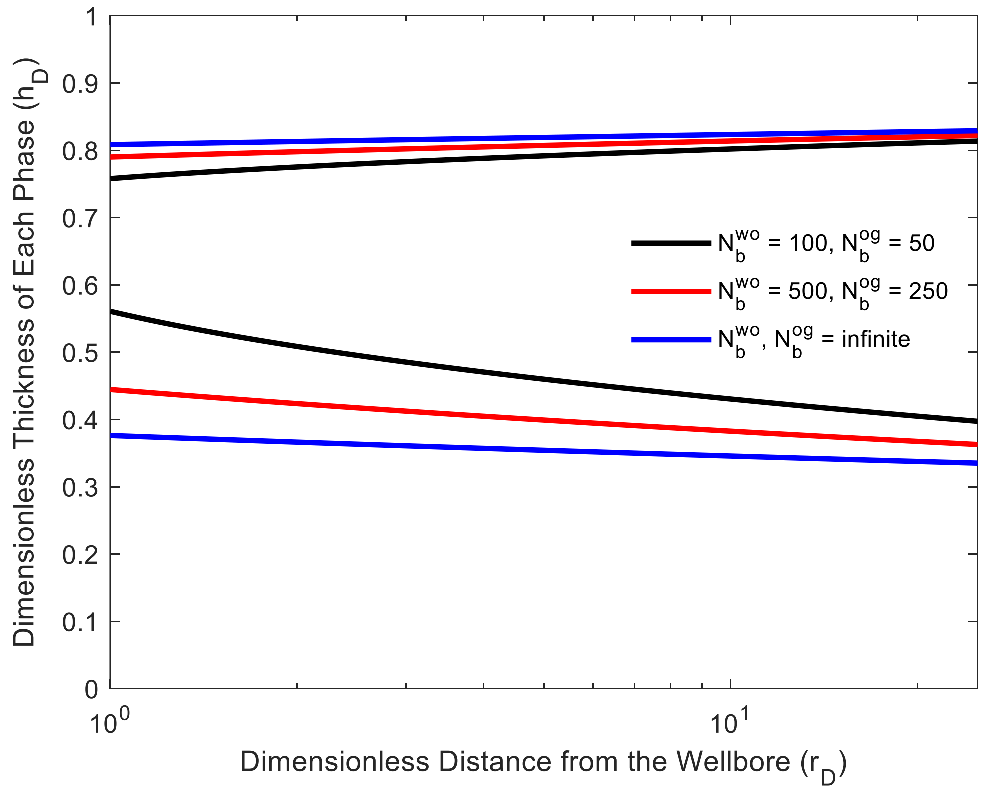

Figure 4.5 Dimensionless thickness of each phase along a cross-section of the reservoir while varying the Bond numbers (both N_b^{wo} and N_b^{og}). The black, red, and blue line show the case where ($N_b^{wo} = 100, N_b^{og} = 50$), ($N_b^{wo} = 500, N_b^{og} = 250$), and ($N_b^{wo}, N_b^{og} =$ infinite). Flow rates are $q_{Dw} = 0.6$, $q_{Do} = 0.2$, and $q_{Dg} = 0.4$ for all three cases.

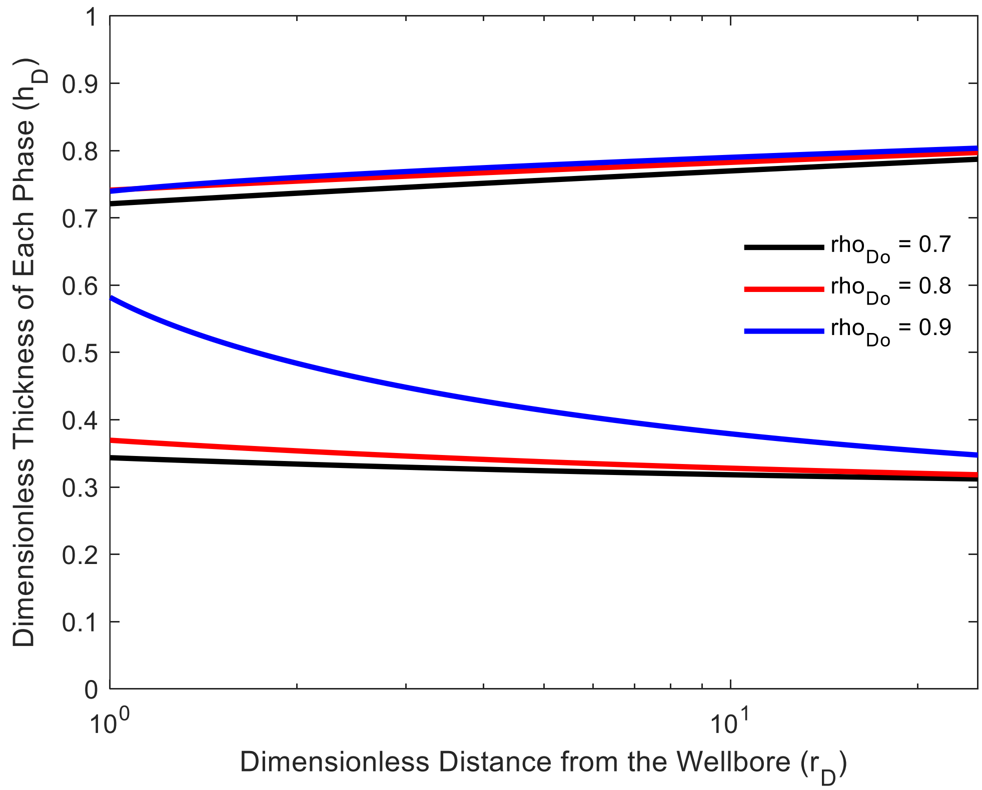

Figure 4.6 Dimensionless thickness of each phase along a cross-section of the reservoir while varying the oil density ratio (ρ_{Do}). The black, red, and blue line show the case where $\rho_{Do} = 0.7$, $\rho_{Do} = 0.8$, and $\rho_{Do} = 0.9$. Flow rates are $q_{Dw} = 0.3$, $q_{Do} = 0.5$, and $q_{Dg} = 0.2$ for all three cases.

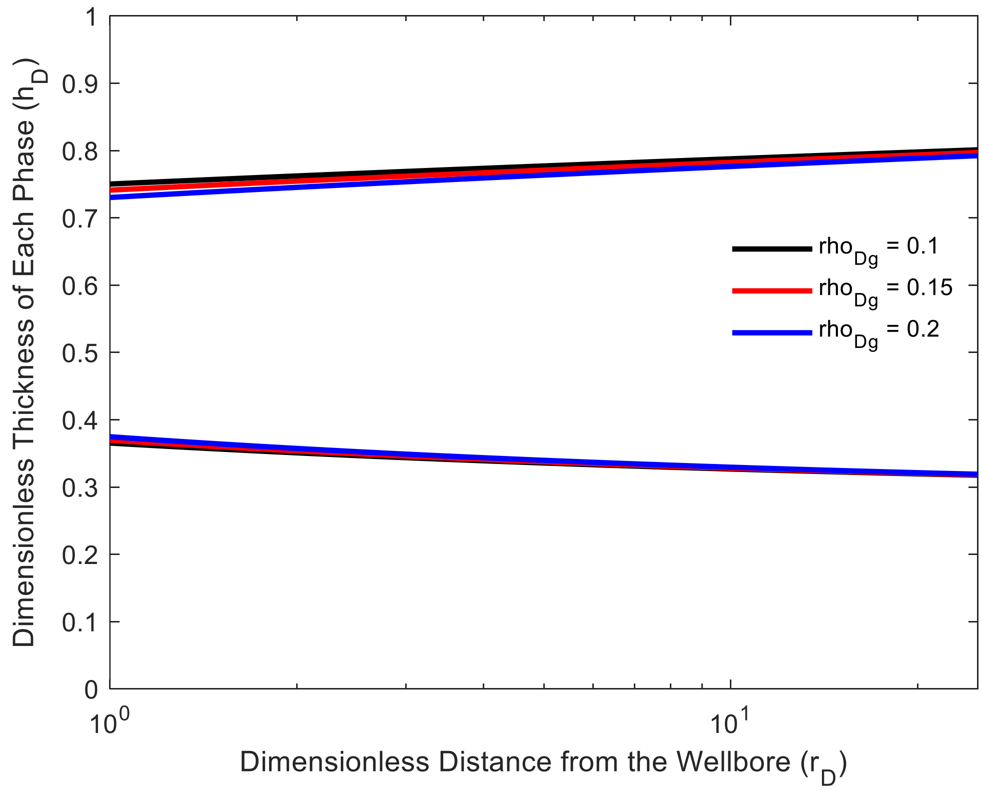

Figure 4.7 Dimensionless thickness of each phase along a cross-section of the reservoir while varying the gas density ratio (ρ_{Dg}). The black, red, and blue line show the case where $\rho_{Dg} = 0.1$, $\rho_{Dg} = 0.15$, and $\rho_{Dg} = 0.2$. Flow rates are $q_{Dw} = 0.3$, $q_{Do} = 0.5$, and $q_{Dg} = 0.2$ for all three cases.

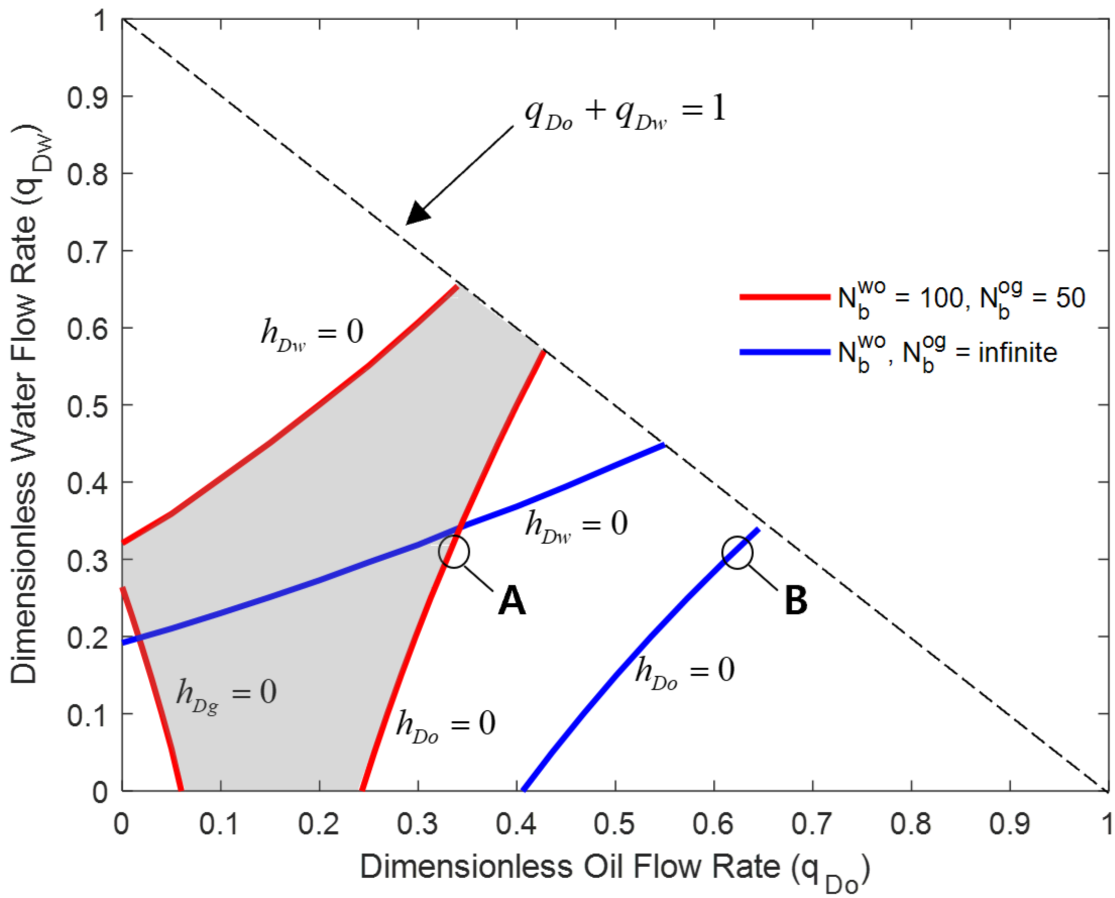

Figure 4.8 Inflow performance windows with physical operating phase rates at constant total rate. The red lines show the boundaries of the physical region where capillary pressure is included ($N_b^{wo} = 100$, $N_b^{og} = 50$) while the blue lines show the boundaries where capillary pressure is neglected (N_b^{wo} and N_b^{og} are infinite). The dashed line shows the case where $q_{Dw} + q_{Do} = 1$ and $q_{Dg} = 0$. The physical operating region with capillary pressure is shown by the gray-colored region. Point A and B shows the critical oil rates where capillary pressure is included and neglected, respectively, as shown in Figure 4.1.

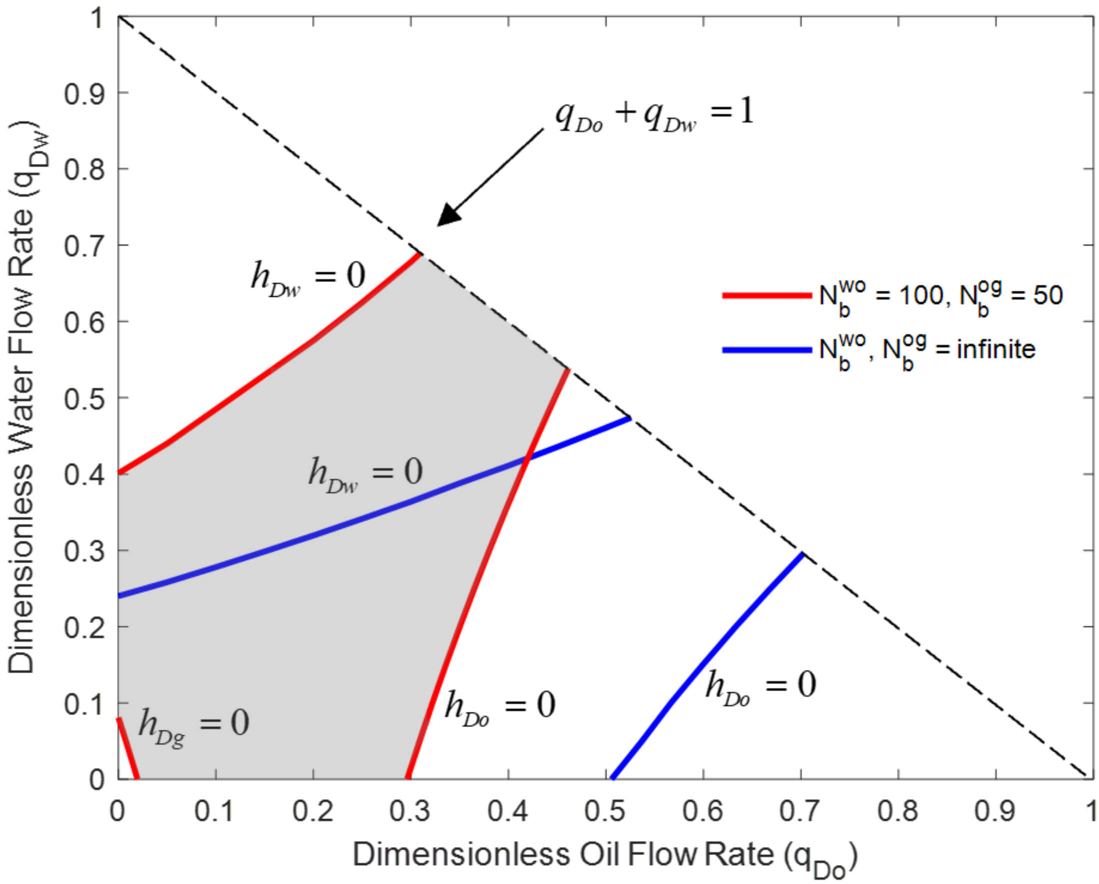

Figure 4.9 Inflow performance windows with physical operating phase rates at constant total rate. Figure 4.9 shows the IPW where both Gravity numbers are increased compared to that of the IPW in Figure 4.8. The red lines show the boundaries of the physical region where capillary pressure is included ($N_b^{wo} = 100,\ N_b^{og} = 50$) while the blue lines show the boundaries where capillary pressure is neglected (N_b^{wo} and N_b^{og} are infinite). The dashed line shows the case where $q_{Dw} + q_{Do} = 1$ and $q_{Dg} = 0$. The physical operating region with capillary pressure is shown by the gray-colored region.

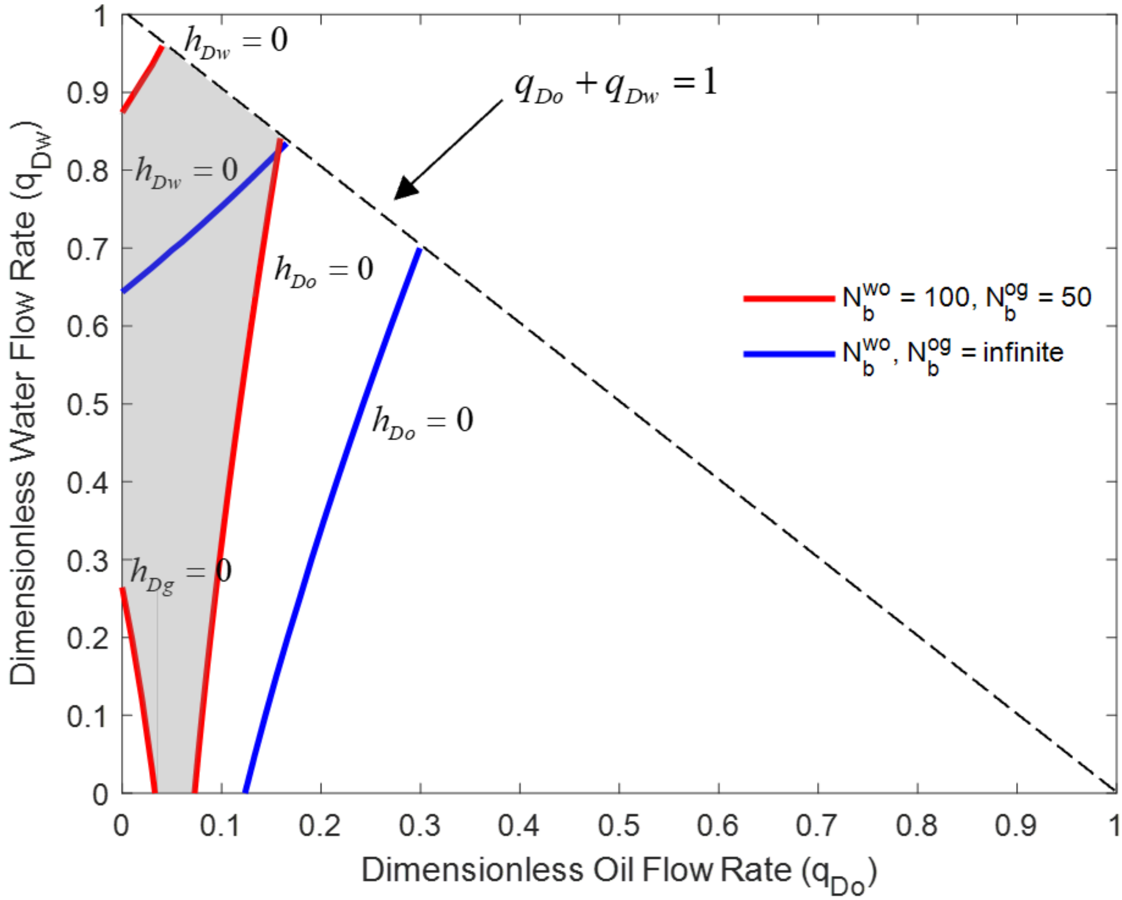

Figure 4.10 Inflow performance windows with physical operating phase rates at constant total rate. Dimensionless oil thickness is decreased compared to that of Figure 4.8. The red lines show the boundaries of the physical region where capillary pressure is included ($N_b^{wo} = 100,\ N_b^{og} = 50$) while the blue lines show the boundaries where capillary pressure is neglected (N_b^{wo} and N_b^{og} are infinite). The dashed line shows the case where $q_{Dw} + q_{Do} = 1$ and $q_{Dg} = 0$. The physical operating region with capillary pressure is shown by the gray-colored region.

Chapter 5

RESULTS FOR MULTIPLE WELL CASE

In this chapter, we give multiple well solutions for several different patterns to demonstrate the superposition function. First, we show a single well with one no-flow boundary (case 2) and a single well with two no-flow boundaries (case 3). Next, we expand the case 3 into two wells with two no-flow boundaries (case 4) and one production well and one injection well in an infinite reservoir (case 5). Last, we show the inverted five-spot pattern in an infinite reservoir (case 6).

5.1 Single well with one no-flow boundary (Case 2)

First, we modelled a case with one production well surrounded by one no-flow boundary in an infinite acting reservoir, as shown in Figure 5.1. The dimensionless area ($r_D \times r_D$) of the reservoir is 500×500. One image well is needed to model the one no-flow boundary, making a total of two wells. The well is located at $(x_D,\ y_D) = (125, 125)$. The boundary condition here is $h_{Dwe} = 0.3$, $h_{Doe} = 0.55$ (and $h_{Dge} = 0.15$) at (x_{De}, $y_{De}) = (500, 500)$.

Figure 5.2 shows the contour map of the dimensionless oil thickness where capillary pressure is neglected (N_b^{wo} and N_b^{og} are infinite). Critical oil rate (q_{Do}) at both wells are 0.9 while $q_{Dw} = 0.05$ and $q_{Dg} = 0.05$. Figure 5.3 shows the contour map of the dimensionless oil thickness where capillary pressure is included ($N_b^{wo} = 100, N_b^{og} = 50$).

Critical oil rate (q_{Do}) at both wells are 0.566 while $q_{Dw} = 0.05$ and $q_{Dg} = 0.384$. The results show that as capillary pressure is included, the critical oil rate decreases from 0.9 to 0.566, again a factor of about 2.0.

5.2 Single well with two no-flow boundaries (Case 3)

We modelled a case with one production well surrounded by two no-flow boundaries in an infinite acting reservoir, as shown in Figure 5.4. The dimensionless area ($r_D \times r_D$) of the reservoir is 500×500. Three image wells are needed to model the two no-flow boundaries, making a total of four wells. The well is located at $(x_D,\ y_D) = (125, 125)$. The boundary condition here is $h_{Dwe} = 0.3$, $h_{Doe} = 0.55$ (and $h_{Dge} = 0.15$) at $(x_{De},\ y_{De}) = (500, 500)$.

Four different cases are shown from Figure 5.5 to Figure 5.8. Figure 5.5 and Figure 5.6 show the contour map of cases where the oil rate is critical in both wells. Figure 5.5 shows the contour map of the dimensionless oil thickness where capillary pressure is neglected (N_b^{wo} and N_b^{og} are infinite). Critical oil rate (q_{Do}) at the well is 0.8129 while $q_{Dw} = 0.005$ and $q_{Dg} = 0.1821$.

Figure 5.6 shows the case where capillary pressure is included ($N_b^{wo} = 100$ and $N_b^{wo} = 50$). q_{Do} at the well is 0.466 while $q_{Dw} = 0.005$ and $q_{Dg} = 0.484$. As capillary pressure is included, the critical rate for both wells decreased from 0.8129 to 0.466 about a factor of 2.0.

Figure 5.7 shows the case where q_{Dg} is increased while q_{Dw} is fixed. q_{Do} at both wells is 0.7, while $q_{Dw} = 0.005$ and $q_{Dg} = 0.295$. Comparison of Figure 5.5 and Figure 5.7 show that increased q_{Dg} results in an increase in the oil thickness.

Figure 5.8 shows the case where q_{Dw} is increased while q_{Dg} is fixed. q_{Do} at both wells is 0.7, while $q_{Dw} = 0.295$ and $q_{Dg} = 0.005$. Comparison of Figure 5.5 and Figure 5.8 show that increased q_{Dw} results in an increase in the oil thickness.

Figure 5.9 shows the estimated critical oil rate from the analytical solution as a function of the dimensionless distance of the well location to the no-flow boundaries. $x_D = y_D$ is assumed for the well location for all cases. Result shows that as the well location is located further from the no-flow boundaries, the critical oil rate for the well increases. That is, the no-flow boundaries affect the production well by decreasing the critical oil rate. Four example cases are shown from Figure 5.10 to Figure 5.13. For all four cases, q_{Dw} is fixed to see the effect of the critical oil rate.

Figure 5.10 shows the case where the well location is $(x_D,\ y_D) = (10,\ 10)$. Critical oil rate for this case is $q_{Do} = 0.4505$ while $q_{Dw} = 0.005$ and $q_{Dg} = 0.5445$. Figure 5.11 shows the case where the well location is $(x_D,\ y_D) = (20,\ 20)$. Critical oil rate for this case is $q_{Do} = 0.5135$ while $q_{Dw} = 0.005$ and $q_{Dg} = 0.4815$. Figure 5.12 shows the case where the well location is $(x_D,\ y_D) = (50,\ 50)$. Critical oil rate for this case is $q_{Do} = 0.6292$ while $q_{Dw} = 0.005$ and $q_{Dg} = 0.3658$. Figure 5.13 shows the case where the well location is $(x_D,\ y_D) = (100,\ 100)$. Critical oil rate for this case is $q_{Do} = 0.7587$ while $q_{Dw} = 0.005$ and $q_{Dg} = 0.2363$.

5.3 Two wells with two no-flow boundaries (Case 4)

We modelled a case with two wells surrounded by no-flow boundaries in an infinite acting reservoir, as shown in Figure 5.14. The dimensionless area ($r_D \times r_D$) of the reservoir is 500×500. We show a quarter of the reservoir in the figure owing to symmetry, where six image wells are needed to model the two no-flow boundaries (making a total of eight wells). The first well is located at $(x_{D1},\ y_{D1}) = (100, 150)$ while the other one is at $(x_{D2},\ y_{D2}) = (150, 100)$, where the intersection of the two perpendicular no-flow boundaries is set at the origin. The boundary condition here is $h_{Dwe} = 0.3$, $h_{Doe} = 0.55$ (and $h_{Dge} = 0.15$) at $(x_{De},\ y_{De}) = (500, 500)$. In this case, both wells are assumed to produce at exactly the same phase rates.

Figures 5.15 to 5.18 show four different cases with varying flow rates. Figure 5.15 shows the contour map of the dimensionless oil phase thickness where capillary pressure is neglected (both N_b^{wo} and N_b^{og} are infinite), and the oil rate is critical and equal to 0.9, while q_{Dw} is 0.05 and q_{Dg} is 0.05. Figure 5.16 shows the case where capillary pressure is included ($N_b^{wo} = 100, N_b^{og} = 50$). As capillary pressure is included, the critical rate for both wells decreased from 0.9 to 0.5, again a factor of about 2.0. Figure 5.17 shows the case where q_{Dg} is increased, which caused the oil thickness to increase. q_{Do} at both wells is 0.8 for this case (critical oil rate), while $q_{Dw} = 0.05$ and $q_{Dg} = 0.15$. Figure 5.18 shows the case where q_{Dw} is increased. The oil thickness increases as q_{Dw} increases. The critical oil flow rate, q_{Do}, at both wells is 0.8, while $q_{Dw} = 0.15$ and $q_{Dg} = 0.05$.

5.4 One production well and one injection well in an infinite reservoir (Case 5)

In this case, we show one production well and one injection well. First, from Figures 5.19 to 5.20, only water is being injected at the injection well. Results show that dimensionless oil thickness decreases while the dimensionless water thickness increases at the injection well.

From Figures 5.21 to 5.24, we operate the one production well and the one injection well at the same time. Figure 5.21 shows the dimensionless oil phase thickness of the case where the boundary condition is $h_{Dwe} = 0.5$, $h_{Doe} = 0.35$, and $h_{Dge} = 0.15$ at (x_{De}, $y_{De}) = (500, 500)$. The critical rate at the production well for this case is 0.436. Figure 5.22 shows the dimensionless water phase thickness.

Figure 5.23 shows the dimensionless oil phase thickness of the case where the boundary condition is $h_{Dwe} = 0.3$, $h_{Doe} = 0.55$, and $h_{Dge} = 0.15$ at $(x_{De},\ y_{De}) = (500, 500)$. The critical rate at the production well for this case is 0.827. Comparison of Figure 5.21 and Figure 5.23 shows that as the dimensionless oil thickness increases, the critical oil rate increases as well. Figure 5.24 shows the dimensionless water thickness.

5.5 Inverted five-spot pattern in an infinite reservoir (Case 6)

Nine square inverted five-spot patterns in an infinite reservoir were modelled as shown in Figure 5.25. Twenty five wells were used to model this case (sixteen production and nine injection wells). The dimensionless area ($r_D \times r_D$) of the reservoir is 500×500 where the boundary condition is $h_{Dwe} = 0.3$, $h_{Doe} = 0.55$, and $h_{Dge} = 0.15$ at (x_{De},

$y_{De}) = (500, 500)$. Only a portion of the reservoir (nine patterns) is shown from Figure 5.26 to Figure 5.32.

Injection is implemented by changing the sign of the total flow rate (positive for injection). All production wells are assumed to produce at the same phase flow rates, while the injection well injects only water. Schematic of the pattern for case 6 is shown in Figure 5.25, where the boundaries of the center pattern are in bold. Capillary pressure is neglected (both N_b^{wo} and N_b^{og} are infinite) in this case.

Figures 5.26 to 5.32 show three different results within the same reservoir. Figures 5.26 to 5.28 show the case where the production well operates at $q_{Dw} = 0.8$, $q_{Do} = 0.1$ and $q_{Dg} = 0.1$. Figure 5.26 shows the dimensionless oil phase thickness while Figure 5.28 shows the dimensionless water phase thickness of the same case. Figure 5.27 shows the enlarged figure of the unit cell of Figure 5.26.

Figures 5.29 and 5.30 show the case where q_{Do} at the production well is increased ($q_{Dw} = 0.5$, $q_{Do} = 0.4$, and $q_{Dg} = 0.1$) compared to that of Figure 5.26. Figure 5.29 shows the dimensionless oil phase thickness while Figure 5.30 shows the dimensionless water phase thickness.

Finally, Figures 5.31 and Figure 5.32 show the case where q_{Do} at the production well is increased further ($q_{Dw} = 0.2$, $q_{Do} = 0.7$, and $q_{Dg} = 0.1$). Figure 5.31 shows the dimensionless oil phase thickness while Figure 5.32 shows the dimensionless water phase thickness. The results show thinning of the oil thickness near the production and injection wells.

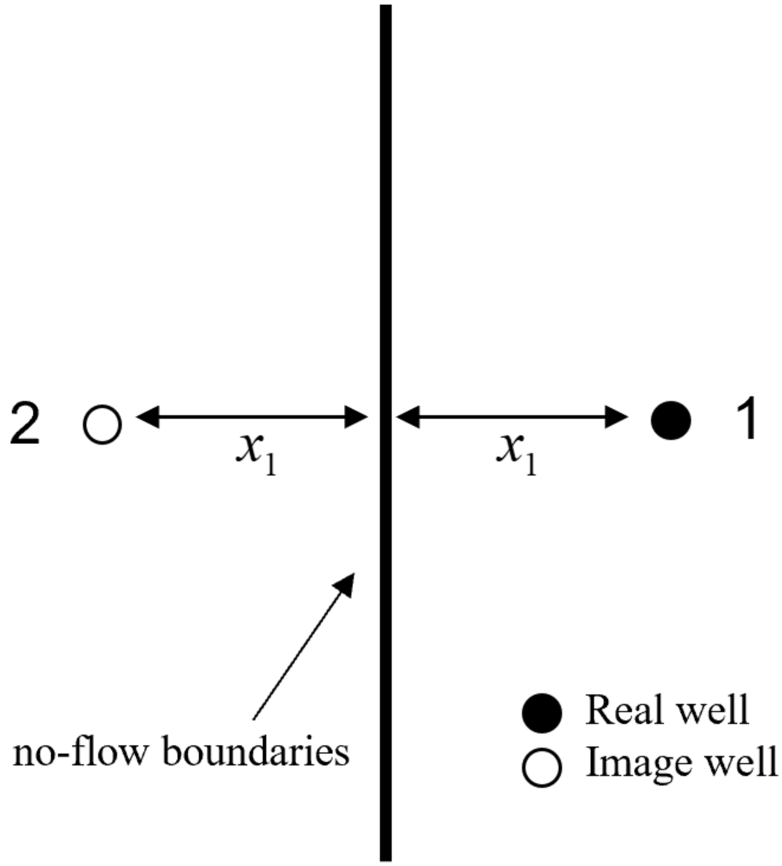

Figure 5.1 Schematic of one well with one no-flow boundary. One production well is located at $(125, 125)$ when the middle point of two wells is at $(0, 125)$. One image well, which is necessary for creation of a no-flow boundary, is shown as well.

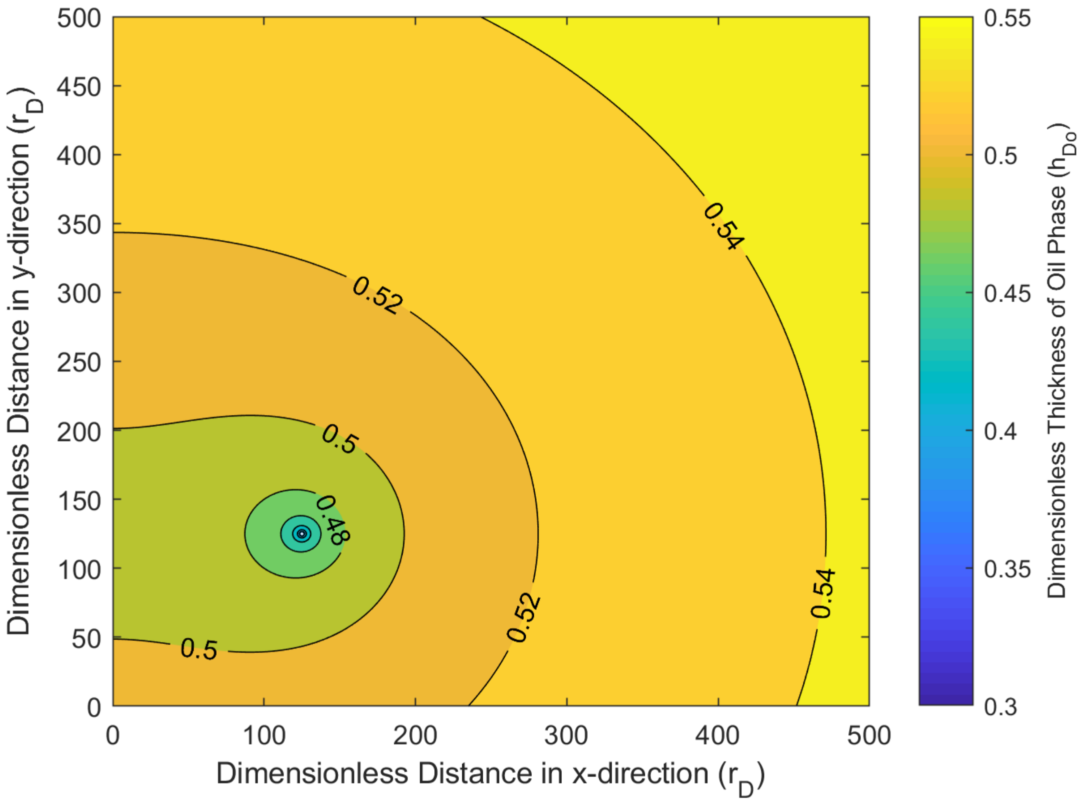

Figure 5.2 Contour map of the dimensionless oil phase thickness estimated from the analytical solution for one well with one no-flow boundary as shown in Figure 5.1. Figure 5.2 shows the case where the oil rate is critical ($q_{Dw} = 0.05, q_{Do} = 0.9, q_{Dg} = 0.05$) and capillary pressure is neglected (N_b^{wo} and N_b^{og} are infinite). Value goes to zero at the well although it is set from 0.3 to 0.55 in order to show the color effect.

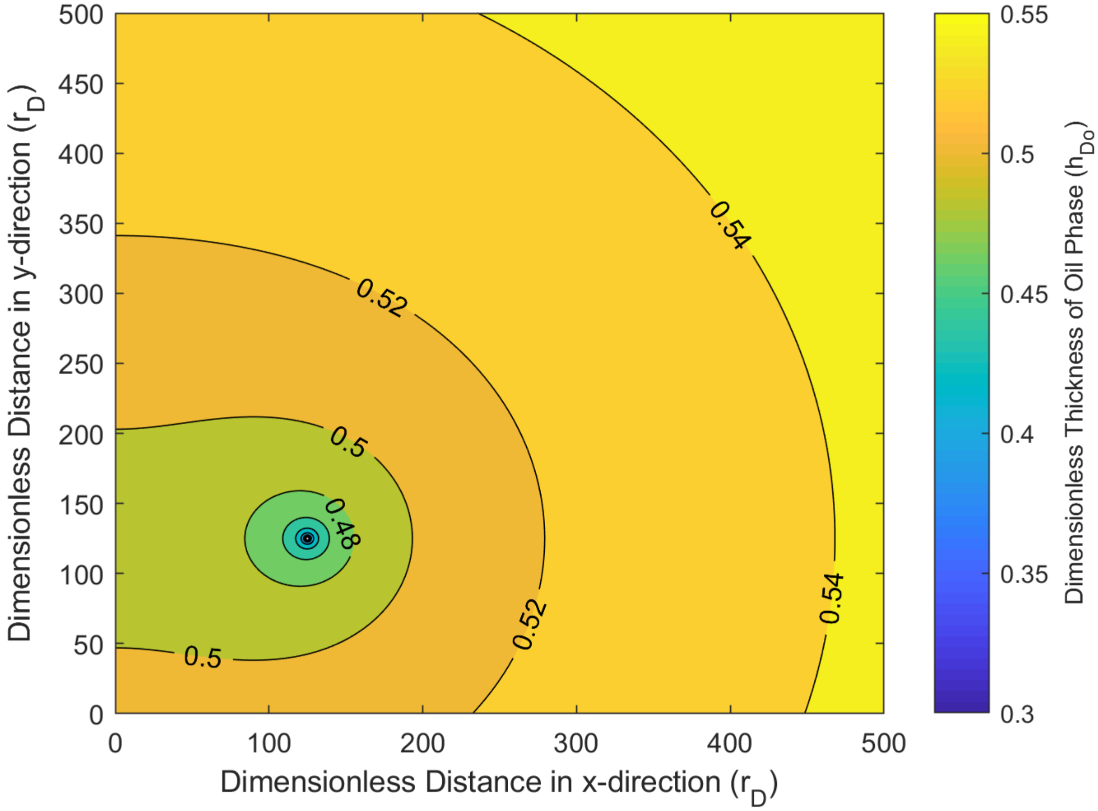

Figure 5.3 Contour map of the dimensionless oil phase thickness estimated from the analytical solution for one well with one no-flow boundary as shown in Figure 5.1. Figure 5.3 shows the case where the oil rate is critical ($q_{Dw} = 0.05, q_{Do} = 0.566, q_{Dg} = 0.384$) and capillary pressure is included ($N_b^{wo} = 100, N_b^{og} = 50$). Value goes to zero at the well although it is set from 0.3 to 0.55 in order to show the color effect.

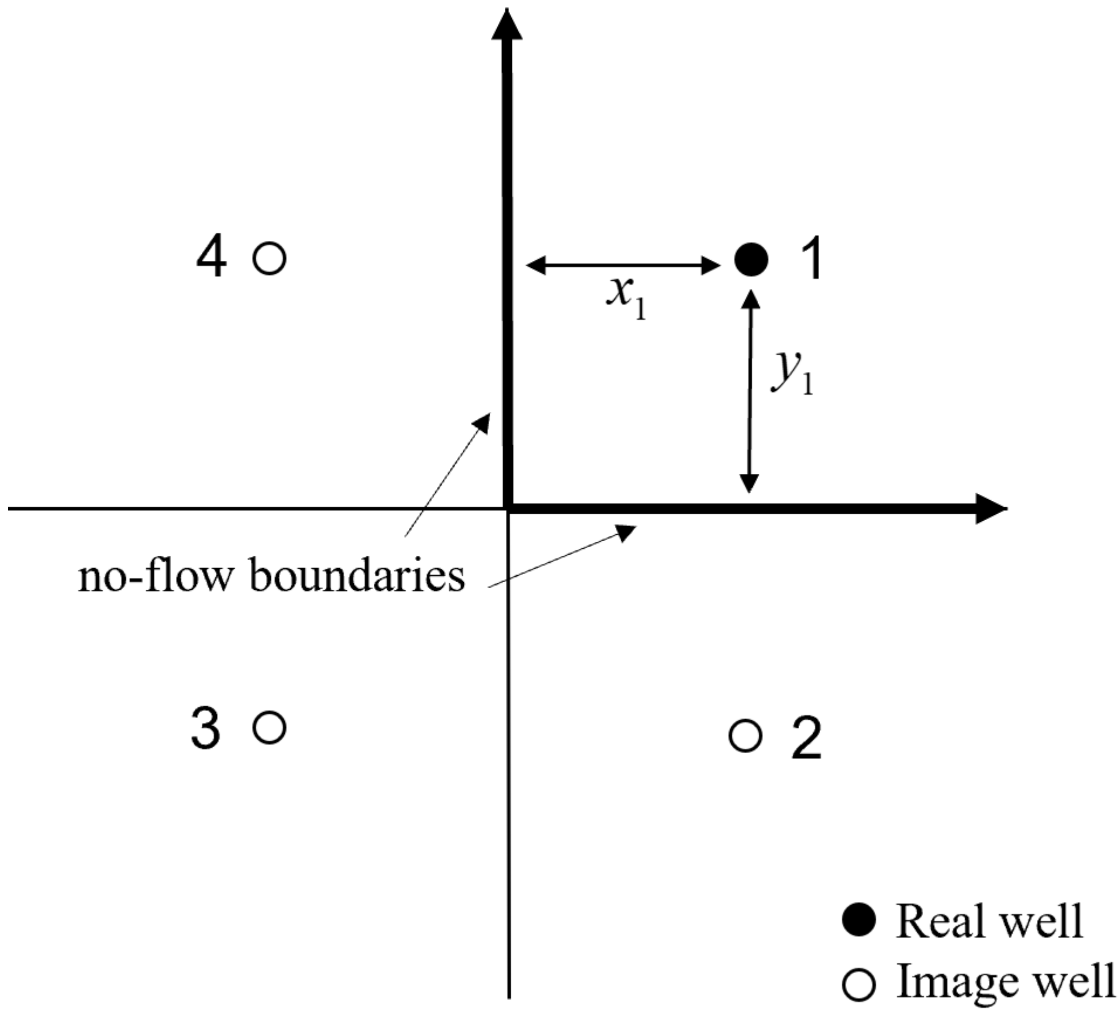

Figure 5.4 Schematic of one well with two no-flow boundaries (after Ansari (2006)). One production well is located at $(125, 125)$ when we set the intersection of two no-flow boundaries to be $(0, 0)$. Three image wells, which are necessary for creation of no-flow boundaries, are shown as well.

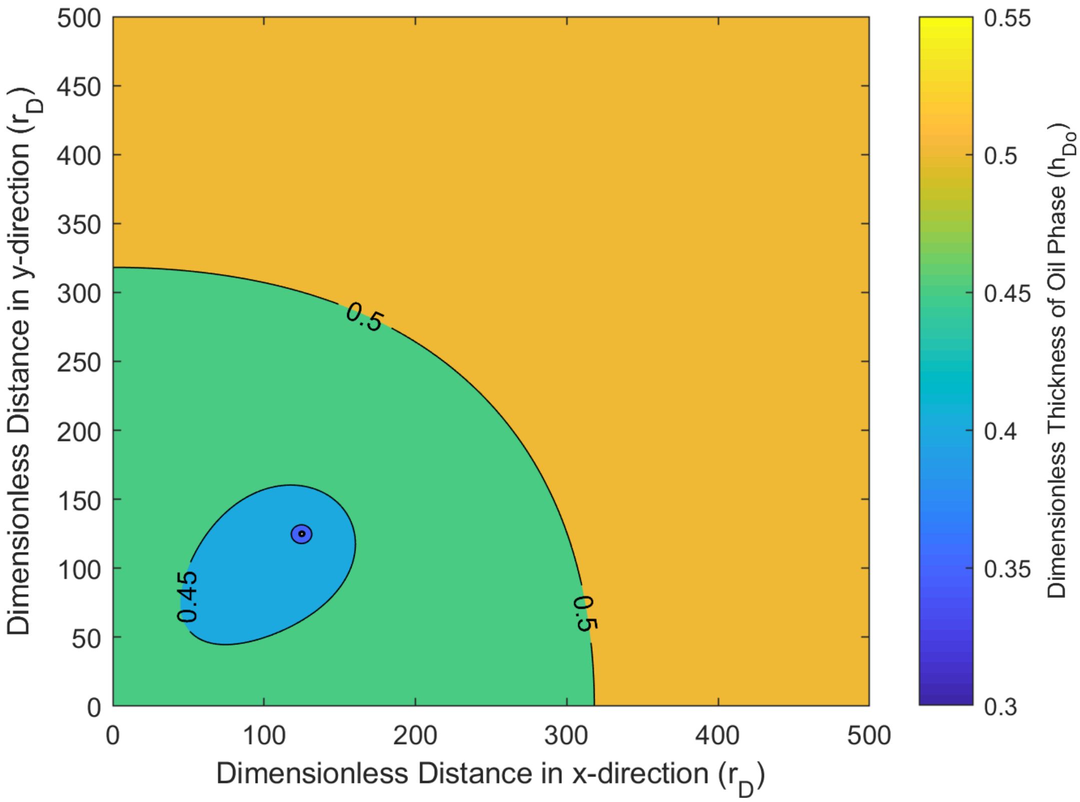

Figure 5.5 Contour map of the dimensionless oil phase thickness estimated from the analytical solution for one well with two no-flow boundaries as shown in Figure 5.4. Figure 5.5 shows the case where the oil rate is critical ($q_{Dw} = 0.005, q_{Do} = 0.8129, q_{Dg} = 0.1821$) and capillary pressure is neglected (N_b^{wo} and N_b^{og} are infinite). Value goes to zero at the well although it is set from 0.3 to 0.55 in order to show the color effect.

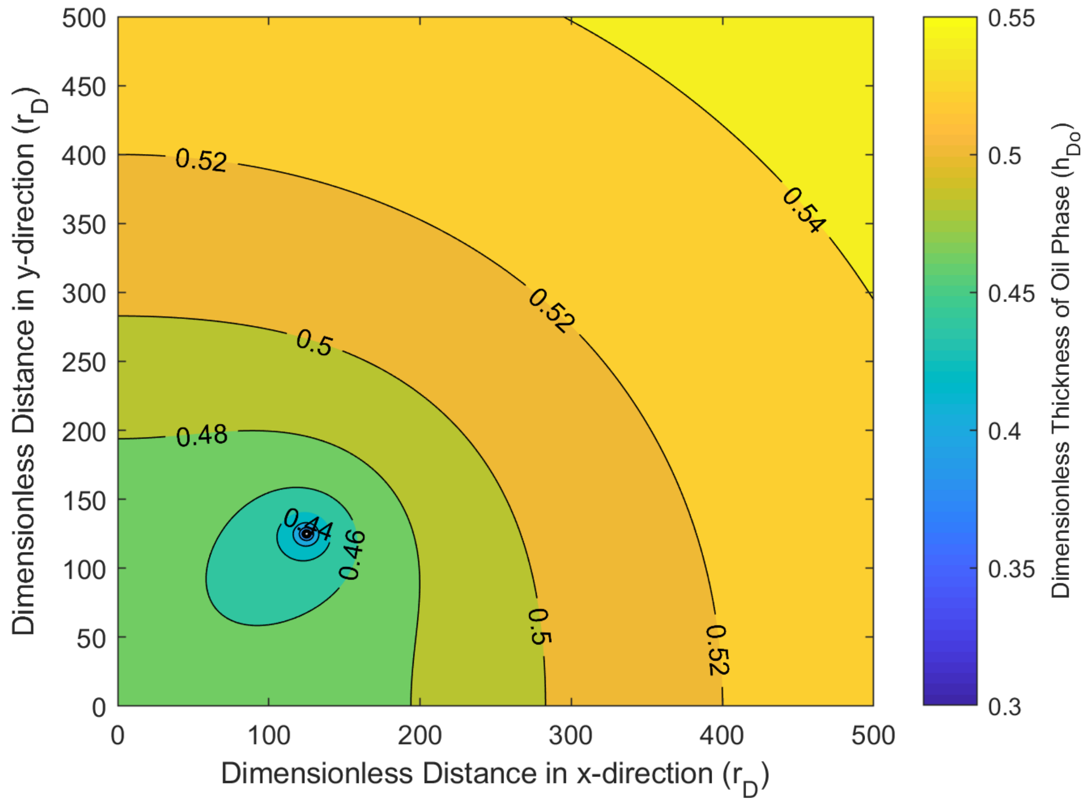

Figure 5.6 Contour map of the dimensionless oil phase thickness estimated from the analytical solution for one well with two no-flow boundaries as shown in Figure 5.4. Figure 5.6 shows the case where the oil rate is critical ($q_{Dw} = 0.005, q_{Do} = 0.466, q_{Dg} = 0.484$) and capillary pressure is included ($N_b^{wo} = 100,\ N_b^{og} = 50$). Value goes to zero at the well although it is set from 0.3 to 0.55 in order to show the color effect.

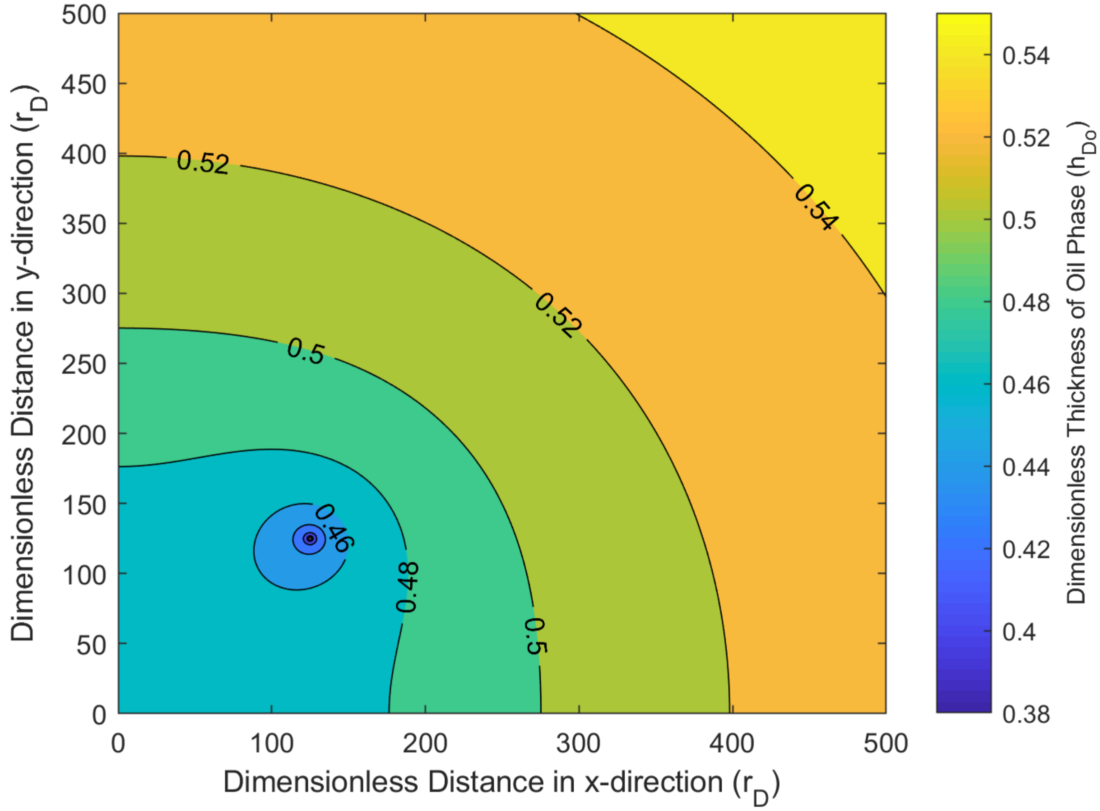

Figure 5.7 Contour map of the dimensionless oil phase thickness estimated from the analytical solution for one well with two no-flow boundaries as shown in Figure 5.4. Figure 5.7 shows the case where q_{Dg} is increased ($q_{Dw} = 0.005, q_{Do} = 0.7, q_{Dg} = 0.295$) compared to that of Figure 5.5.

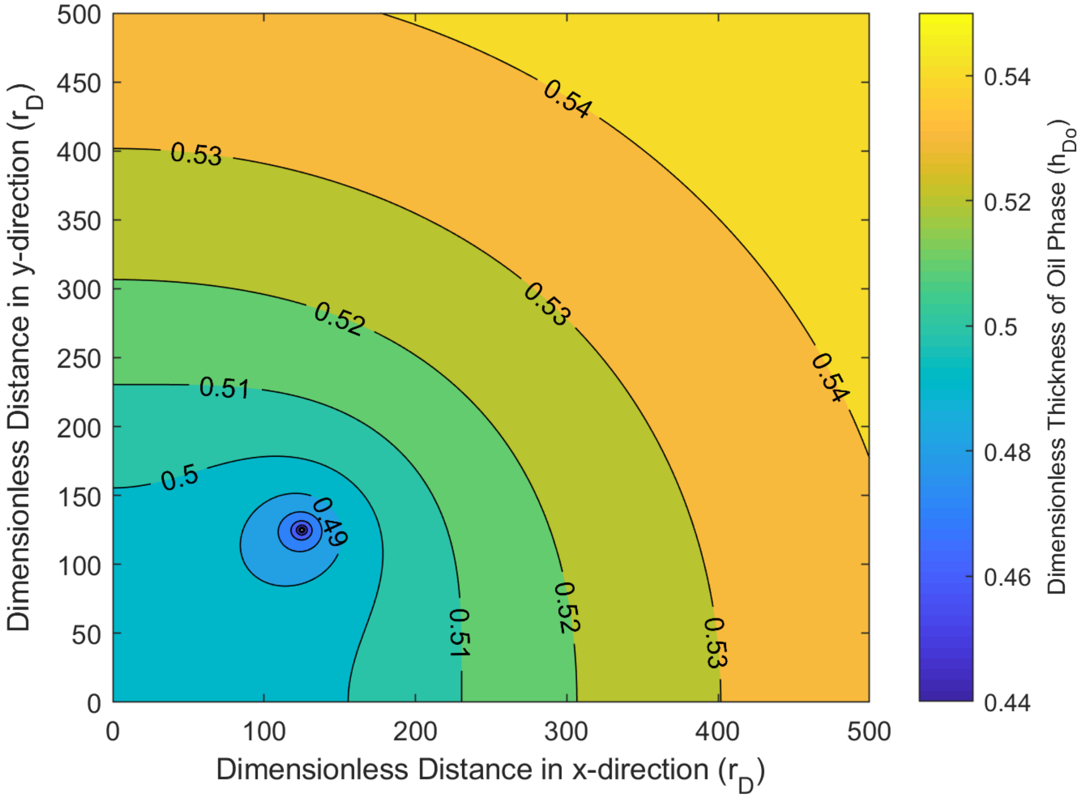

Figure 5.8 Contour map of the dimensionless oil phase thickness estimated from the analytical solution for one well with two no-flow boundaries as shown in Figure 5.4. Figure 5.8 shows the case where q_{Dw} is increased ($q_{Dw} = 0.295, q_{Do} = 0.7, q_{Dg} = 0.005$) compared to that of Figure 5.5

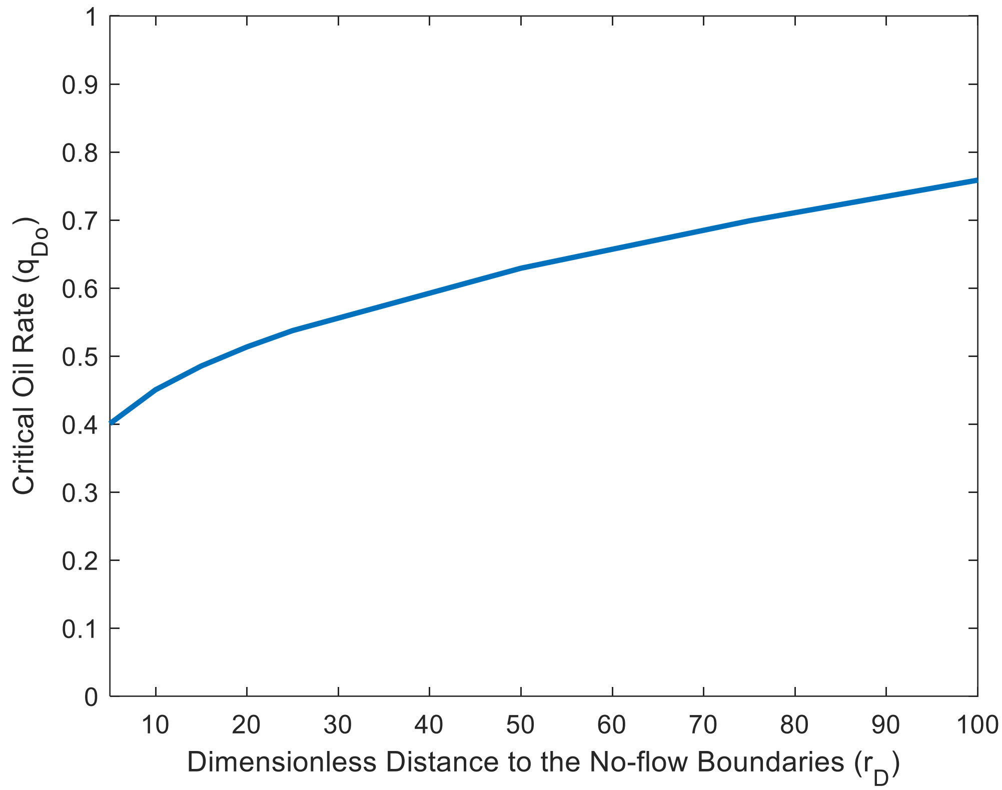

Figure 5.9 Critical oil rate as a function of the dimensionless distance of the well location to the no-flow boundaries of Figure 5.4. For all cases in Figure 5.4, $x_D = y_D$ is assumed for the well location.

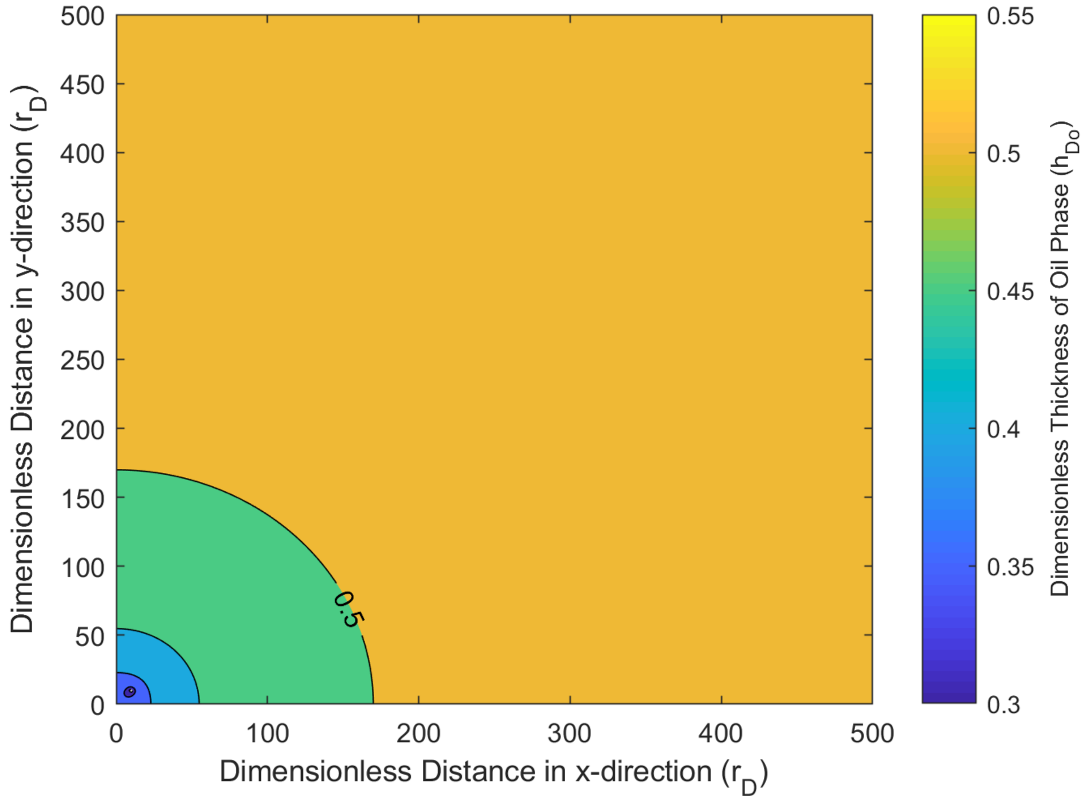

Figure 5.10 Contour map of the dimensionless oil phase thickness estimated from the analytical solution for one well with two no-flow boundaries as shown in Figure 5.4. Figure 5.10 shows the case where the well location is $(x_D,\ y_D) = (10,\ 10)$. Critical oil rate for this case is $q_{Do} = 0.4505$ while $q_{Dw} = 0.005$ and $q_{Dg} = 0.5445$. Value goes to zero at the well although it is set from 0.3 to 0.55 in order to show the color effect.

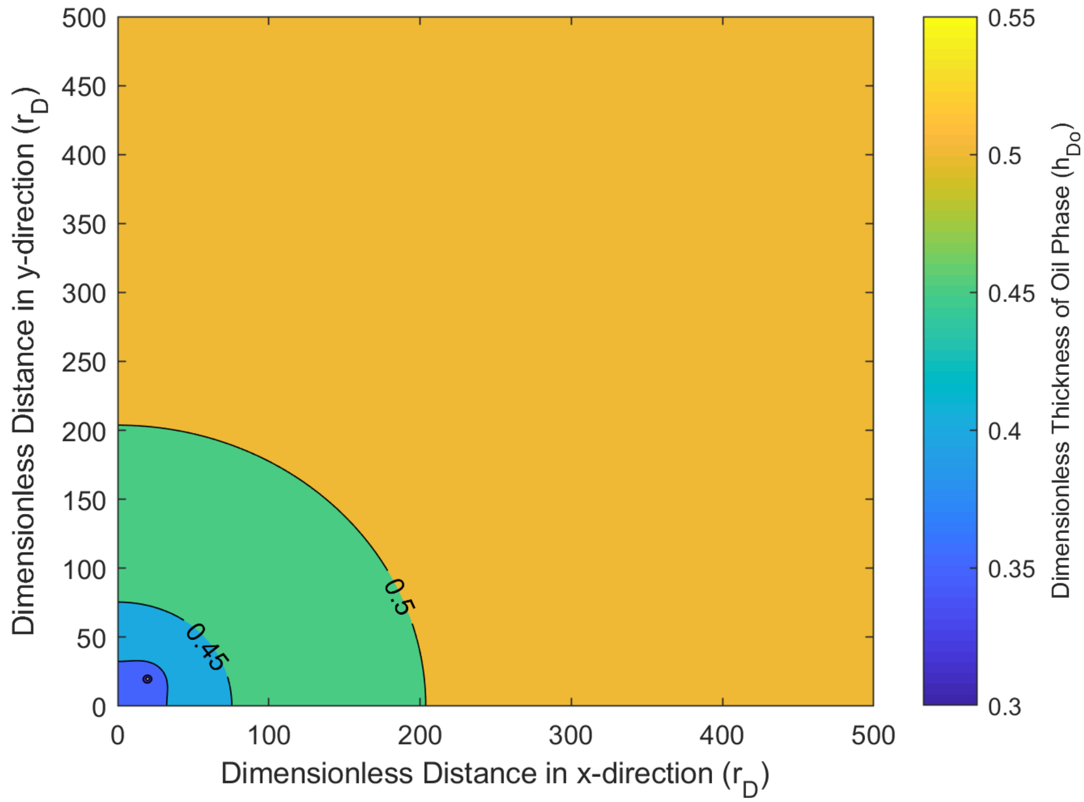

Figure 5.11 Contour map of the dimensionless oil phase thickness estimated from the analytical solution for one well with two no-flow boundaries as shown in Figure 5.4. Figure 5.11 shows the case where the well location is $(x_D,\ y_D) = (20,\ 20)$. Critical oil rate for this case is $q_{Do} = 0.5135$ while $q_{Dw} = 0.005$ and $q_{Dg} = 0.4815$. Value goes to zero at the well although it is set from 0.3 to 0.55 in order to show the color effect.

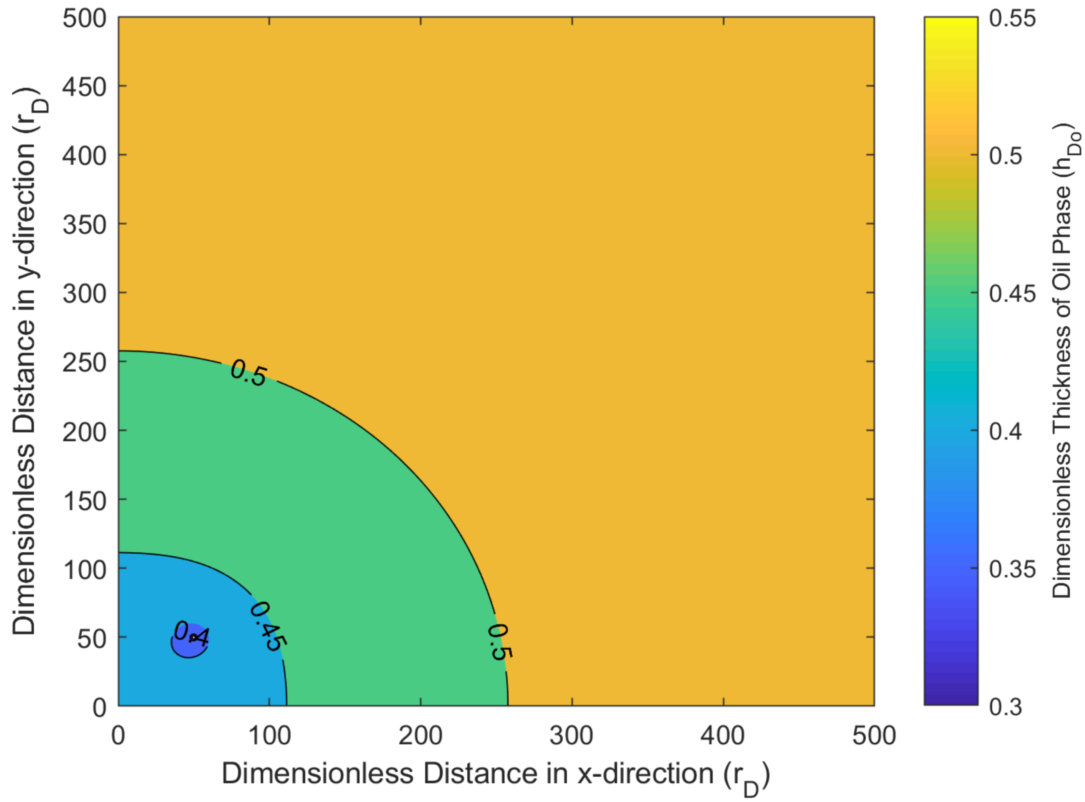

Figure 5.12 Contour map of the dimensionless oil phase thickness estimated from the analytical solution for one well with two no-flow boundaries as shown in Figure 5.4. Figure 5.12 shows the case where the well location is $(x_D,\ y_D) = (50,\ 50)$. Critical oil rate for this case is $q_{Do} = 0.6292$ while $q_{Dw} = 0.005$ and $q_{Dg} = 0.3658$. Value goes to zero at the well although it is set from 0.3 to 0.55 in order to show the color effect.

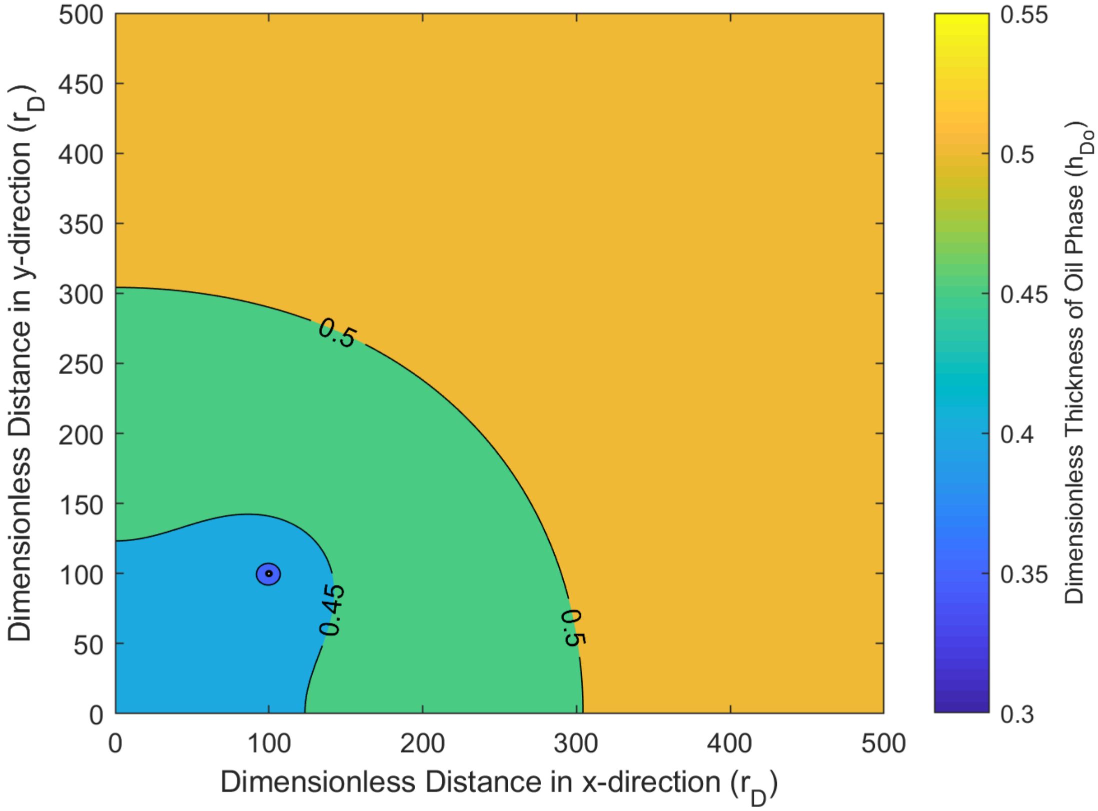

Figure 5.13 Contour map of the dimensionless oil phase thickness estimated from the analytical solution for one well with two no-flow boundaries as shown in Figure 5.4. Figure 5.13 shows the case where the well location is $(x_D,\ y_D) = (100,\ 100)$. Critical oil rate for this case is $q_{Do} = 0.7587$ while $q_{Dw} = 0.005$ and $q_{Dg} = 0.2363$. Value goes to zero at the well although it is set from 0.3 to 0.55 in order to show the color effect.

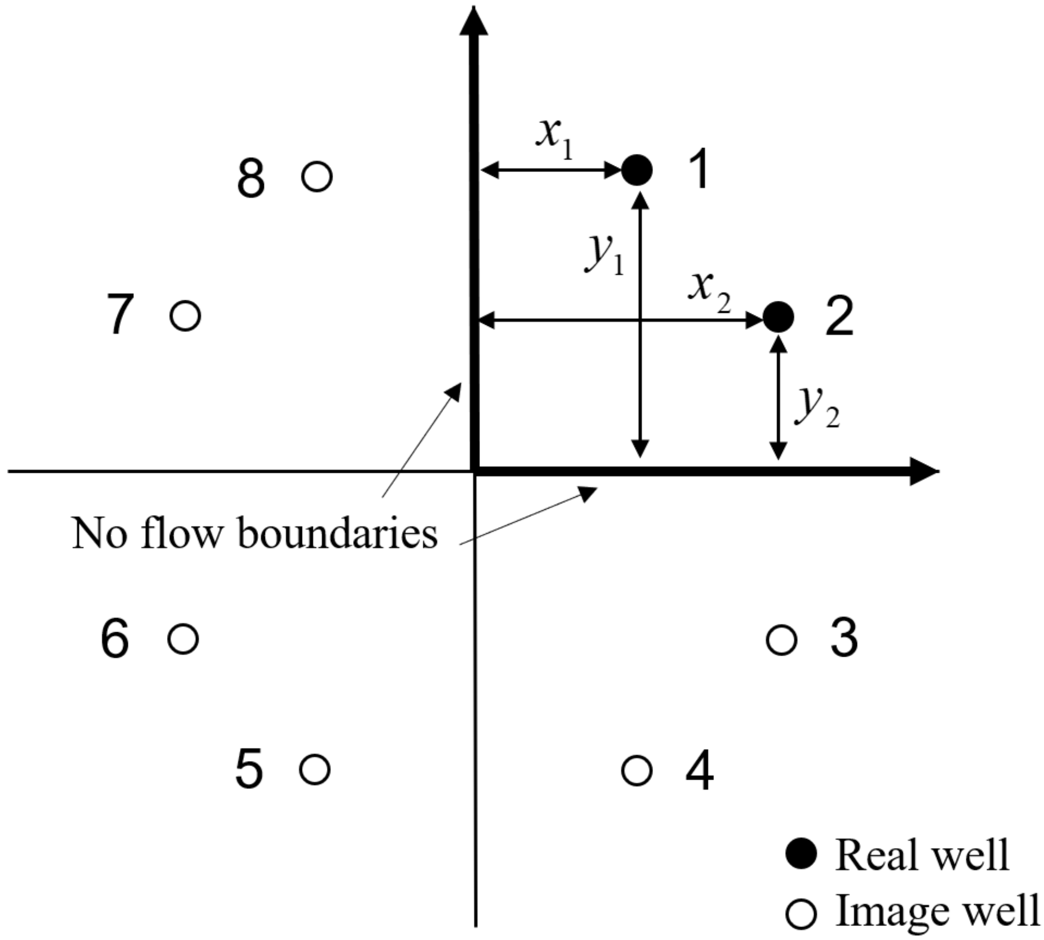

Figure 5.14 Schematic of two wells with two no-flow boundaries (after Ansari (2006)). Two wells are located at $(100, 150)$ and $(150, 100)$ and the intersection of two no-flow boundaries is at $(0, 0)$. Six image wells are necessary for creation of the two no-flow boundaries as shown.

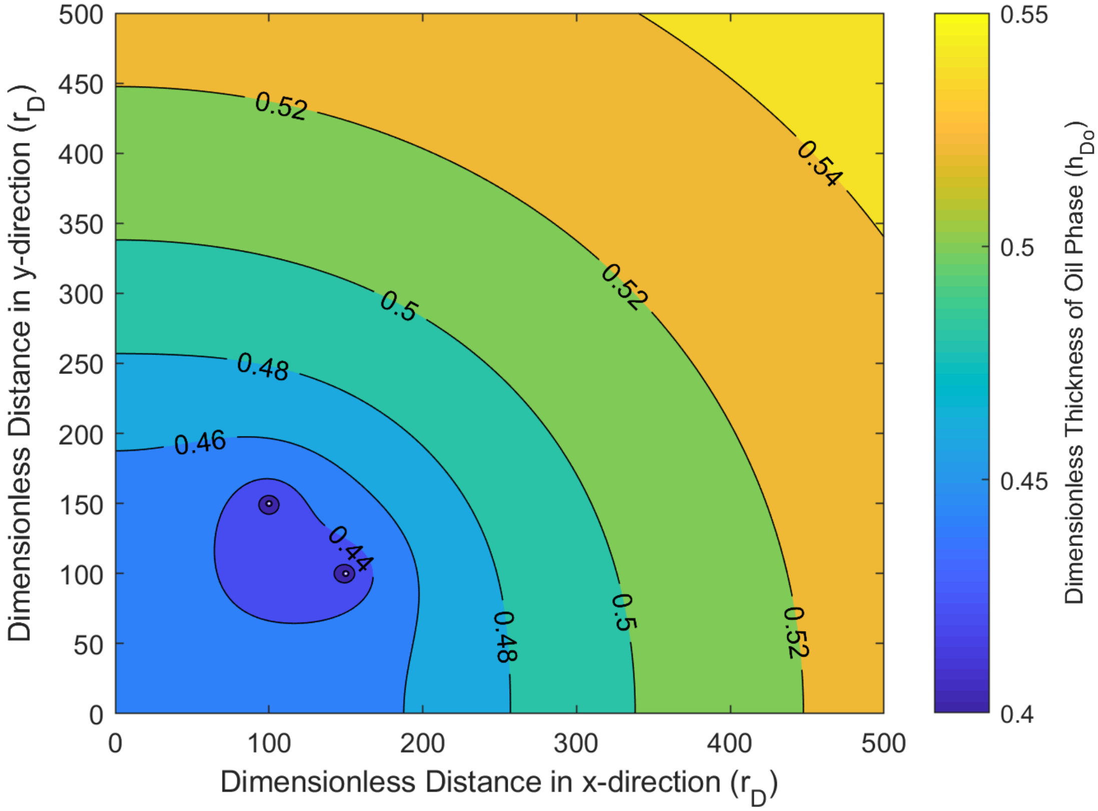

Figure 5.15 Contour map of the dimensionless oil phase thickness estimated from the analytical solution for two wells with two no-flow boundaries as shown in Figure 5.14. Figure 5.15 shows the case where ($q_{Dw} = 0.05, q_{Do} = 0.9, q_{Dg} = 0.05$) and capillary pressure is neglected (N_b^{wo} and N_b^{og} are infinite). Value goes to zero at the well although it is set from 0.4 to 0.55 in order to show the color effect.

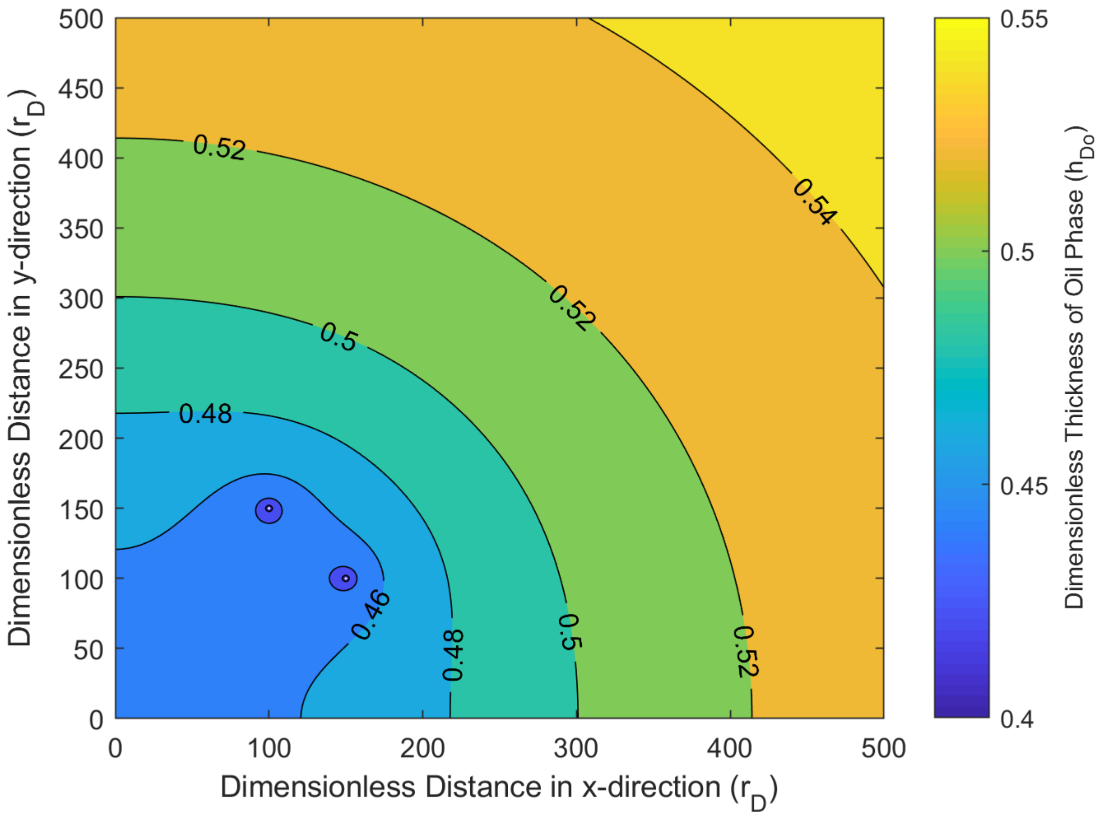

Figure 5.16 Contour map of the dimensionless oil phase thickness estimated from the analytical solution for two wells with two no-flow boundaries as shown in Figure 5.14. Figure 5.16 shows the case where ($q_{Dw} = 0.05, q_{Do} = 0.5, q_{Dg} = 0.45$) and capillary pressure is included ($N_b^{wo} = 100$, $N_b^{og} = 50$). Value goes to zero at the well although it is set from 0.4 to 0.55 in order to show the color effect.

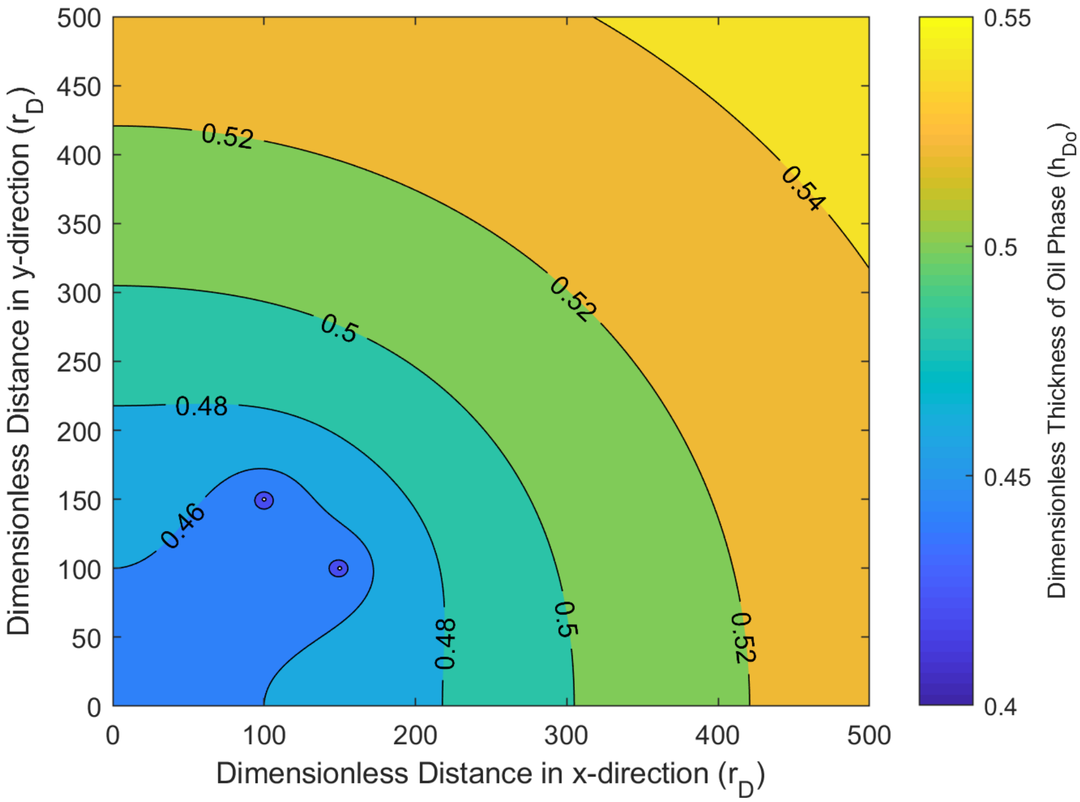

Figure 5.17 Contour map of the dimensionless oil phase thickness estimated from the analytical solution for two wells with two no-flow boundaries as shown in Figure 5.14. Figure 5.17 shows the case where q_{Dg} is increased ($q_{Dw} = 0.05, q_{Do} = 0.8, q_{Dg} = 0.15$) compared to that of Figure 5.15.

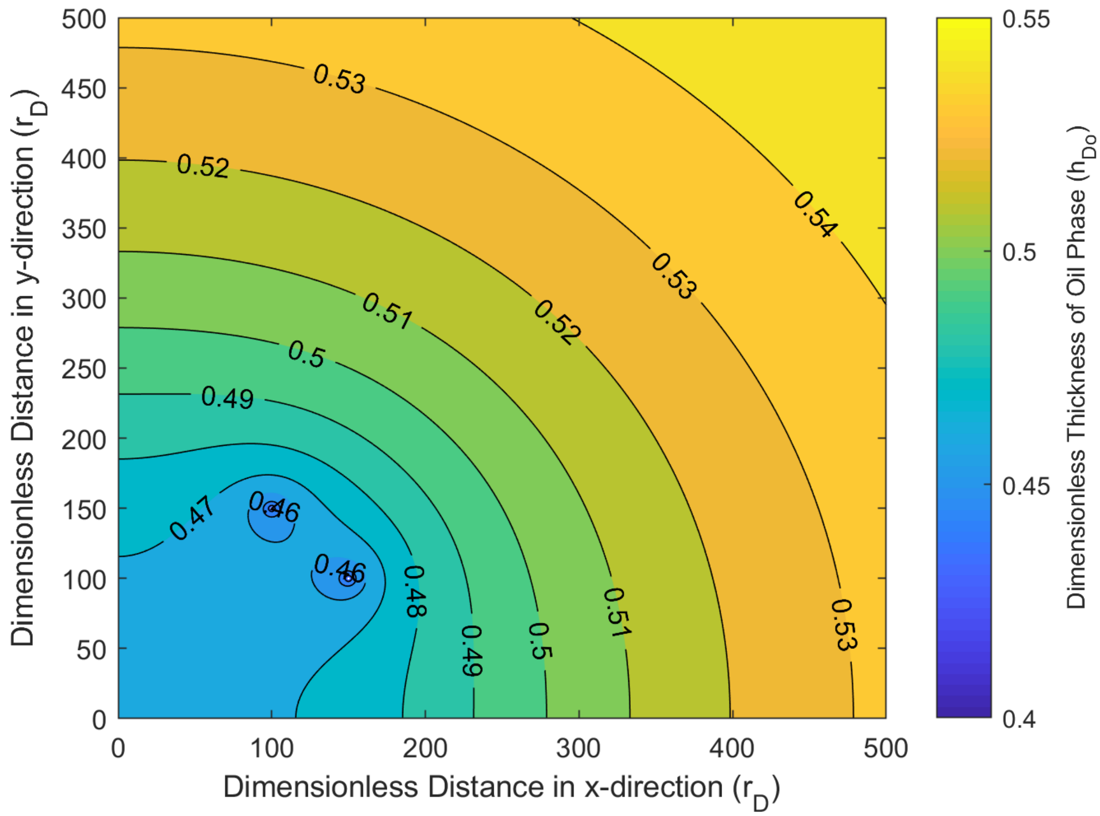

Figure 5.18 Contour map of the dimensionless oil phase thickness estimated from the analytical solution for two wells with two no-flow boundaries as shown in Figure 5.14. Figure 5.18 shows the case where q_{Dw} is increased ($q_{Dw} = 0.15, q_{Do} = 0.8, q_{Dg} = 0.05$) compared to that of Figure 5.15.

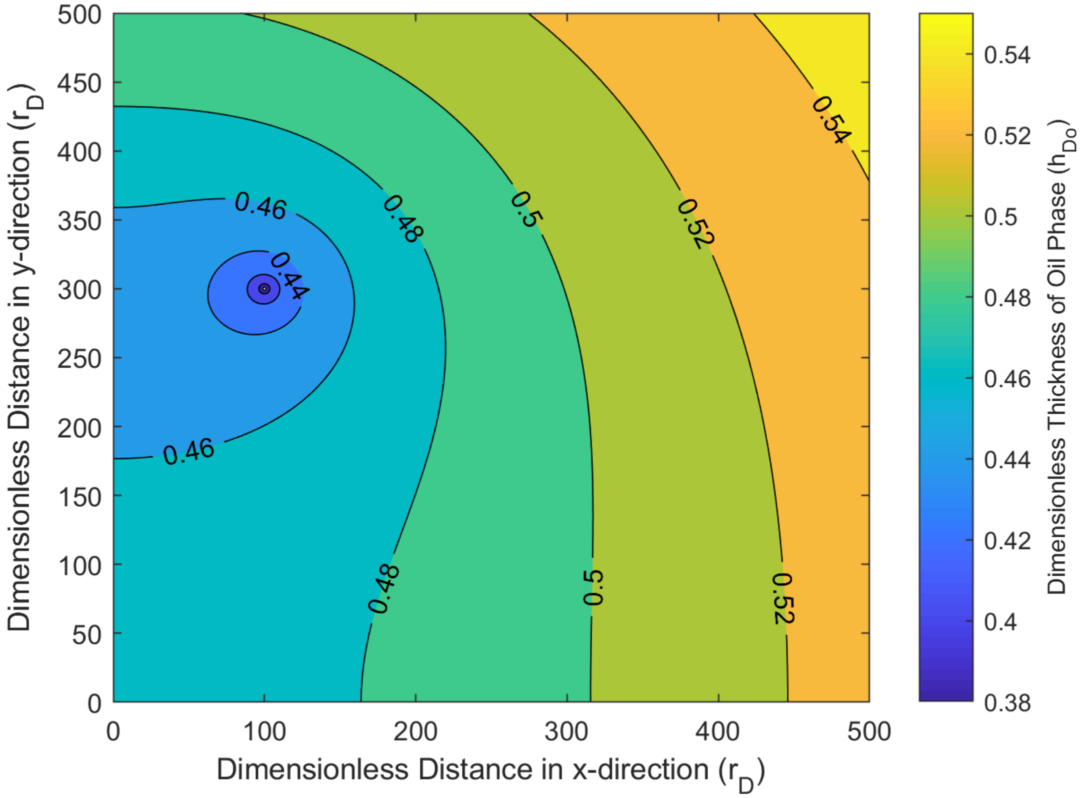

Figure 5.19 Contour map of the dimensionless oil phase thickness estimated from the analytical solution for one injection well with two no-flow boundaries as shown in Figure 5.14. The boundary condition is $h_{Dwe} = 0.3$, $h_{Doe} = 0.55$, and $h_{Dge} = 0.15$ at $(x_{De},\ y_{De}) = (500, 500)$.

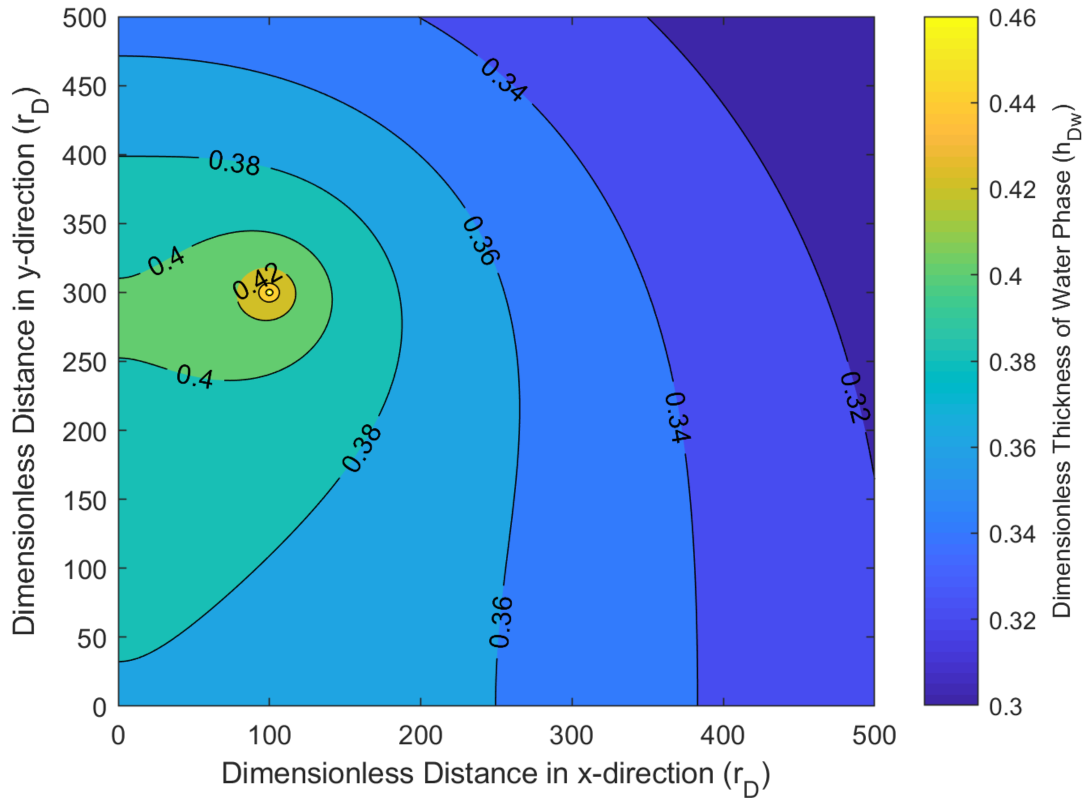

Figure 5.20 Contour map of the dimensionless water phase thickness estimated from the analytical solution for one injection well with two no-flow boundaries as shown in Figure 5.14. The boundary condition is $h_{Dwe} = 0.3$, $h_{Doe} = 0.55$, and $h_{Dge} = 0.15$ at $(x_{De},\ y_{De}) = (500, 500)$.

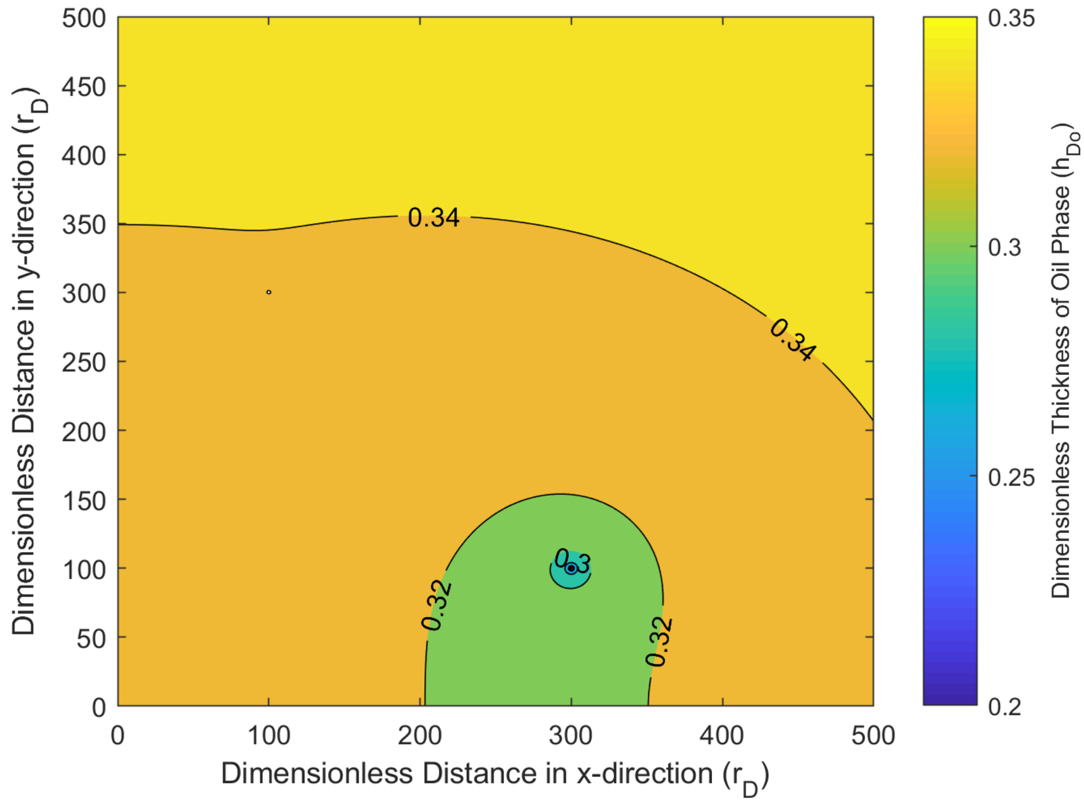

Figure 5.21 Contour map of the dimensionless oil phase thickness estimated from the analytical solution for one injection well and one production well with two no-flow boundaries as shown in Figure 5.14. Figure 5.21 shows the critical oil rate case ($q_{Dw} = 0.479, q_{Do} = 0.471, q_{Dg} = 0.05$) where the boundary condition is $h_{Dwe} = 0.5$, $h_{Doe} = 0.35$, and $h_{Dge} = 0.15$ at $(x_{De},\ y_{De}) = (500, 500)$. Value goes to zero at the well although it is set from 0.2 to 0.35 in order to show the color effect.

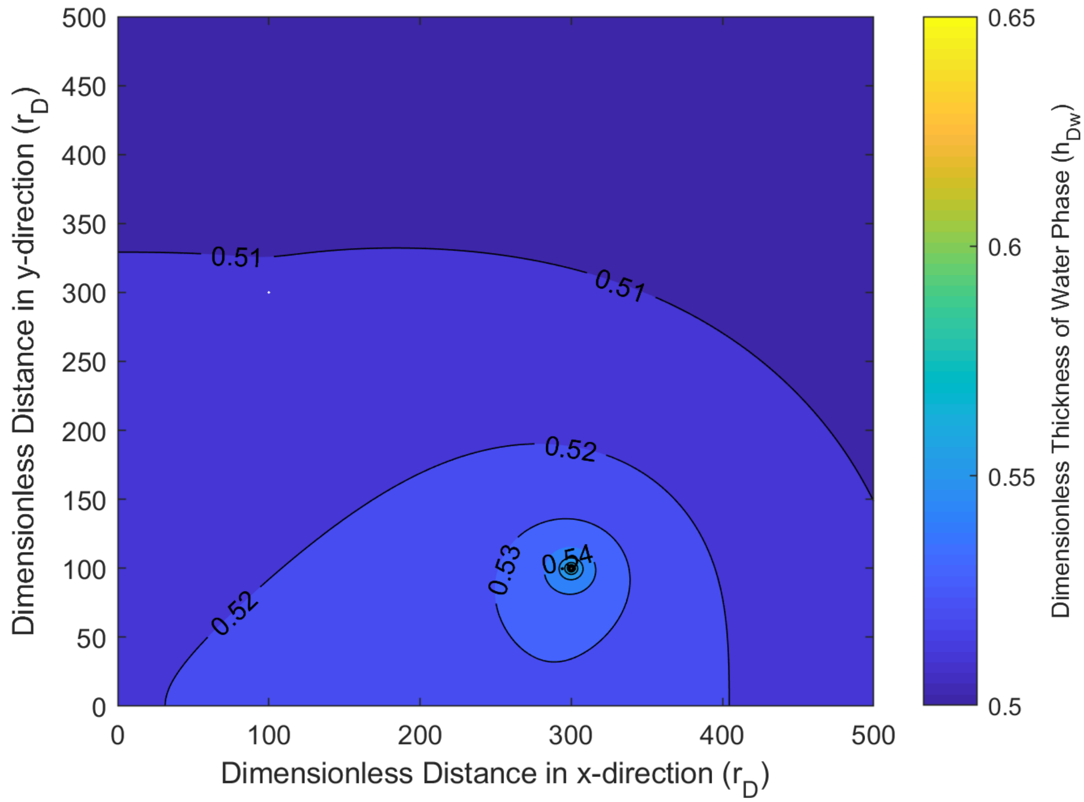

Figure 5.22 Contour map of the dimensionless water phase thickness estimated from the analytical solution for one injection well and one production well with two no-flow boundaries as shown in Figure 5.14. Figure 5.22 shows the critical oil rate case ($q_{Dw} = 0.479, q_{Do} = 0.471, q_{Dg} = 0.05$) where the boundary condition is $h_{Dwe} = 0.5$, $h_{Doe} = 0.35$, and $h_{Dge} = 0.15$ at $(x_{De},\ y_{De}) = (500, 500)$.

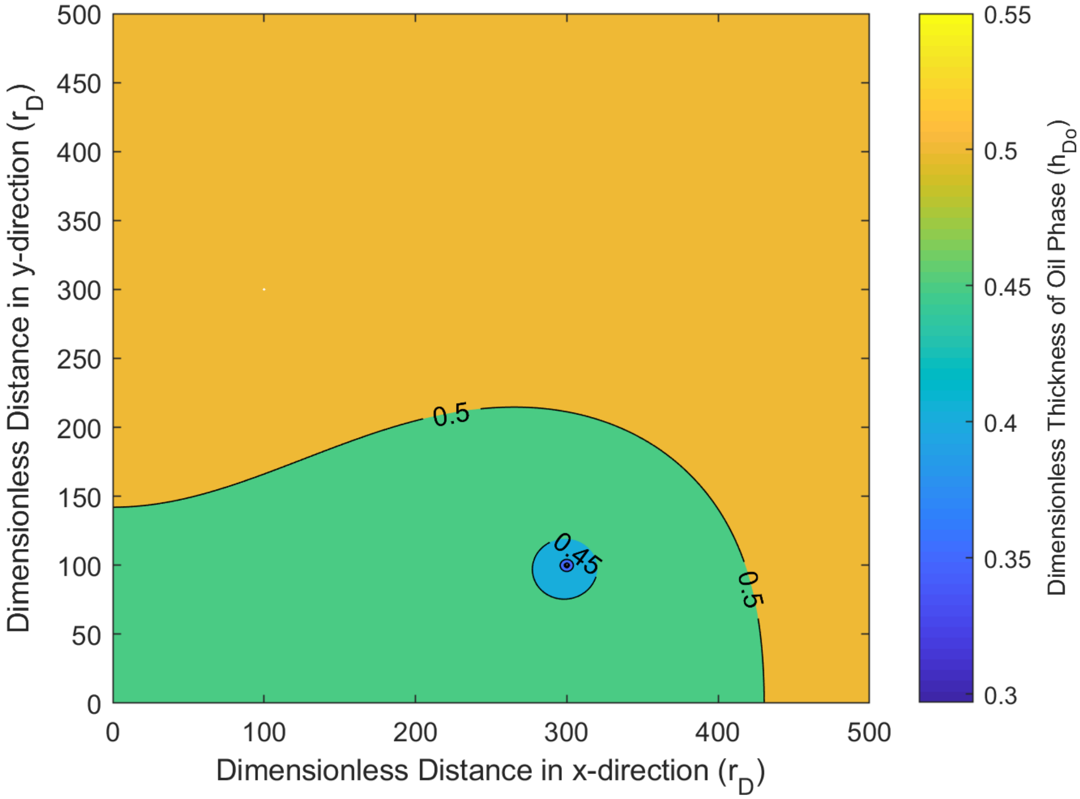

Figure 5.23 Contour map of the dimensionless oil phase thickness estimated from the analytical solution for one injection well and one production well with two no-flow boundaries as shown in Figure 5.14. Figure 5.22 shows the critical oil rate case ($q_{Dw} = 0.093, q_{Do} = 0.902, q_{Dg} = 0.05$) where the boundary condition is $h_{Dwe} = 0.3,\ h_{Doe} = 0.55,$ and $h_{Dge} = 0.15$ at $(x_{De},\ y_{De}) = (500, 500)$. Value goes to zero at the well although it is set from 0.3 to 0.55 in order to show the color effect.

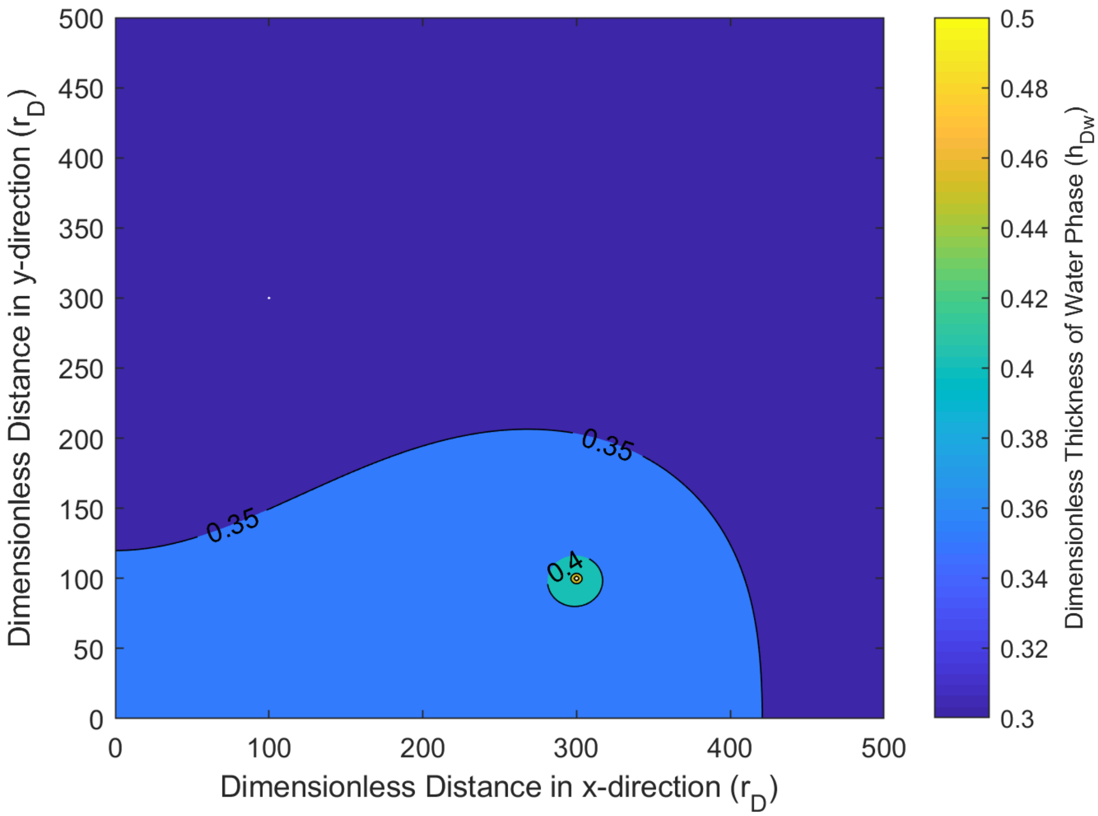

Figure 5.24 Contour map of the dimensionless water phase thickness estimated from the analytical solution for one injection well and one production well with two no-flow boundaries as shown in Figure 5.14. Figure 5.22 shows the critical oil rate case ($q_{Dw} = 0.093, q_{Do} = 0.902, q_{Dg} = 0.05$) where the boundary condition is $h_{Dwe} = 0.3$, $h_{Doe} = 0.55$, and $h_{Dge} = 0.15$ at $(x_{De},\ y_{De}) = (500, 500)$.

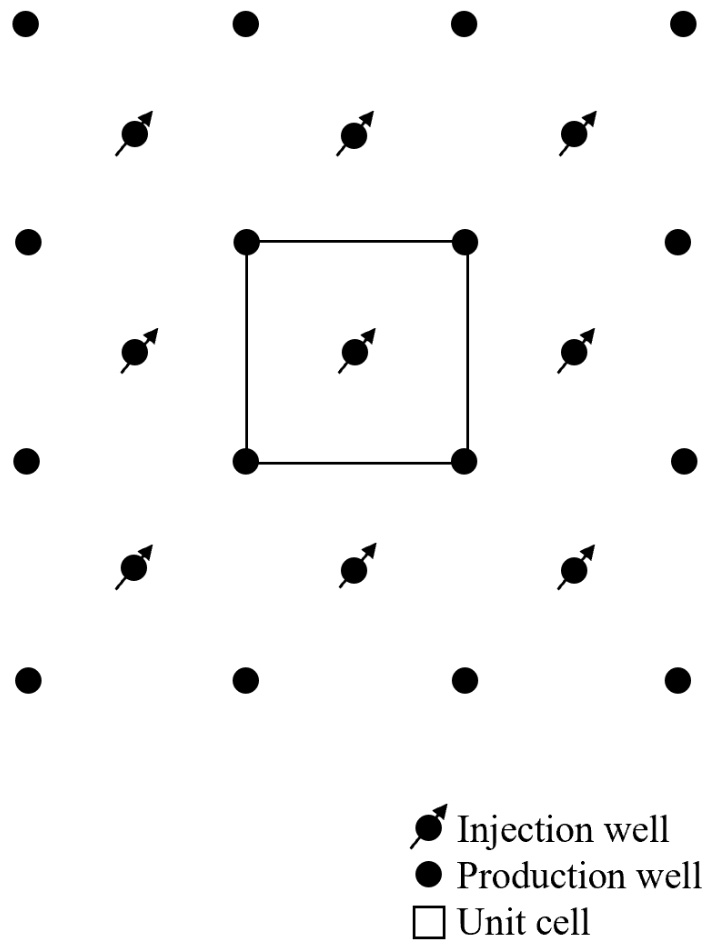

Figure 5.25 Schematic of twenty five wells using a partially confined inverted five-spot pattern in an infinite reservoir.

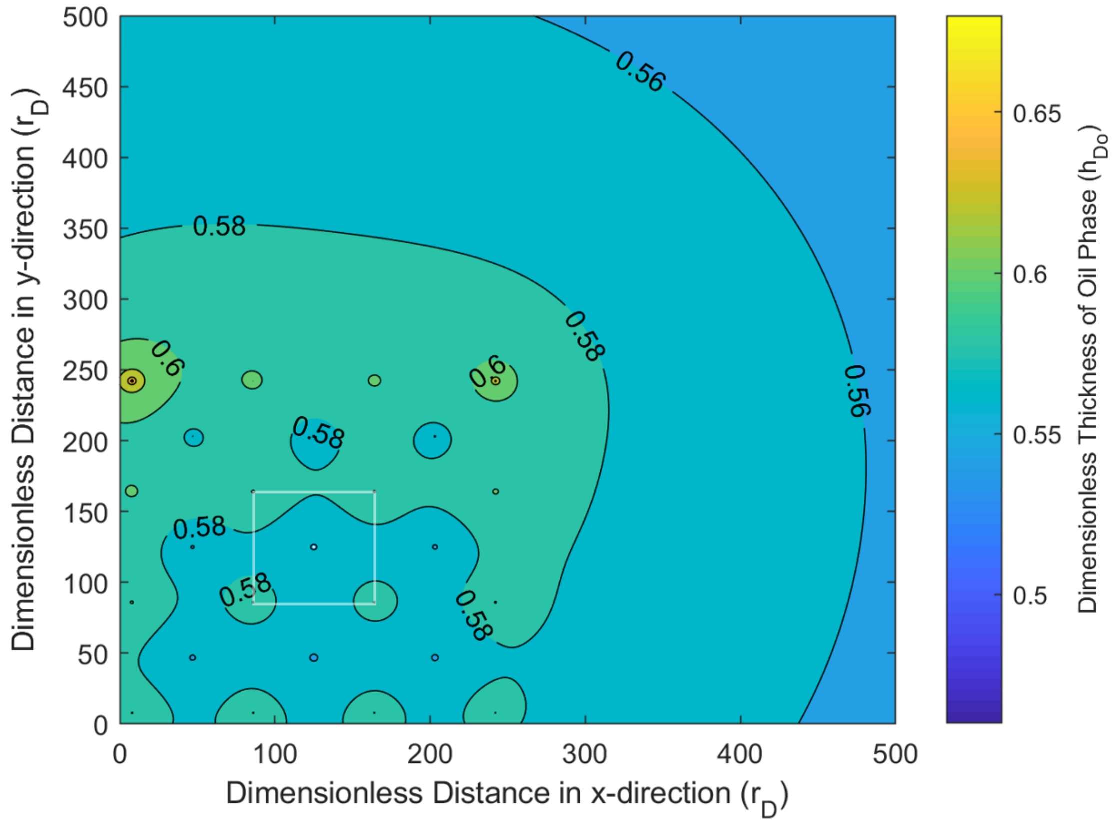

Figure 5.26 Contour map of the dimensionless oil phase thickness for an inverted five-spot pattern as shown in Figure 5.25. Figure 5.26 shows the case with production wells at $q_{Dw} = 0.8, q_{Do} = 0.1, q_{Dg} = 0.1$ and injection wells ($q_{Dw} = 1$). Capillary pressure is neglected (both N_b^{wo} and N_b^{og} are infinite).

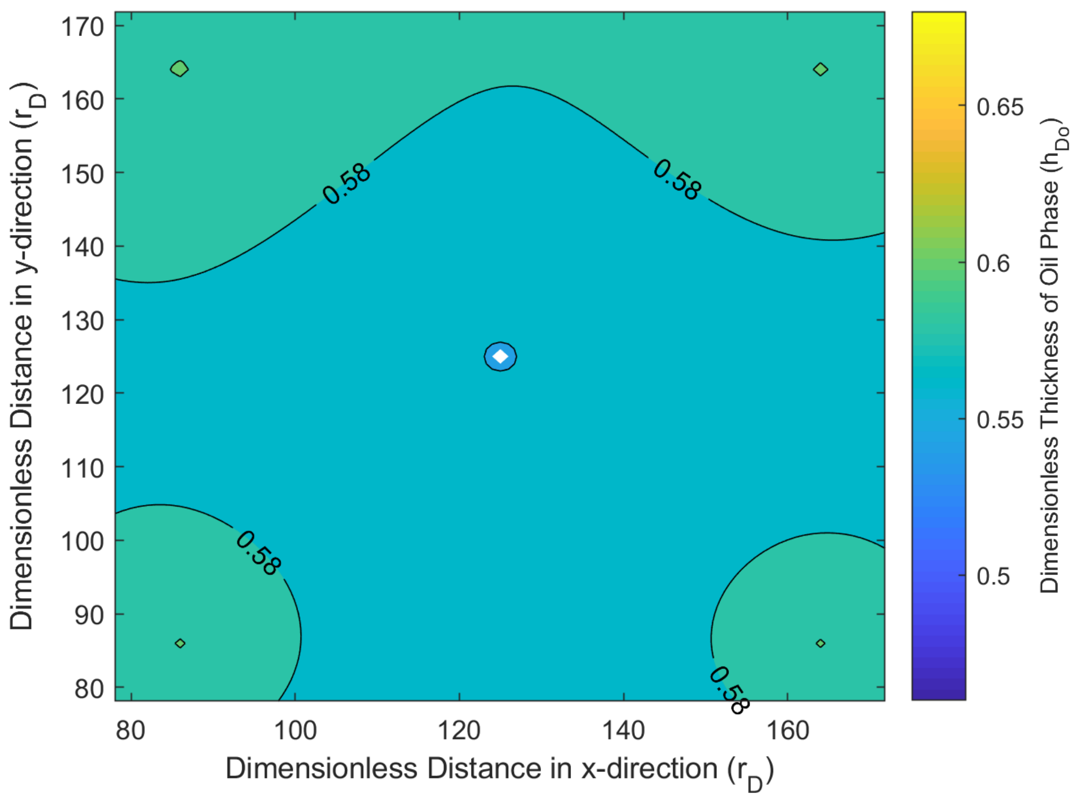

Figure 5.27 Contour map of the dimensionless oil phase thickness for an inverted five-spot pattern as shown in Figure 5.25. Figure 5.27 shows the enlarged figure of the unit cell of Figure 5.26. Capillary pressure is neglected (both N_b^{wo} and N_b^{og} are infinite).

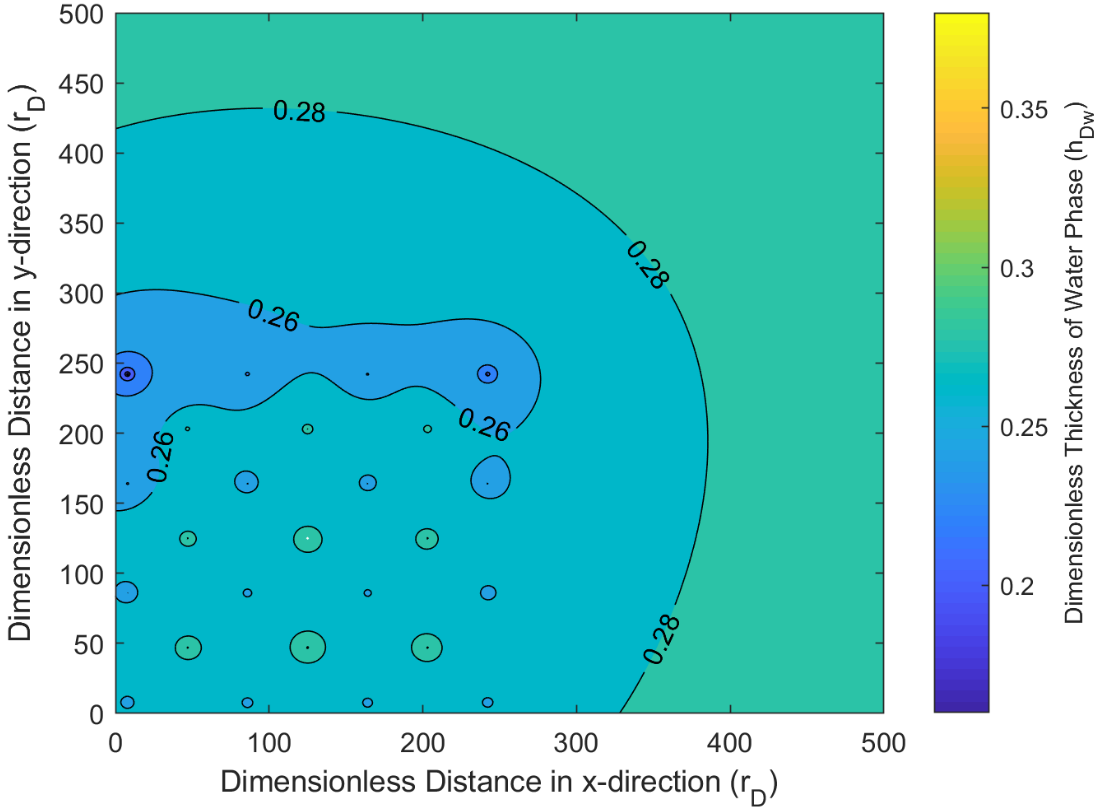

Figure 5.28 Contour map of the dimensionless water phase thickness for an inverted five-spot pattern as shown in Figure 5.25. Figure 5.28 shows the case with production wells at $q_{Dw} = 0.8, q_{Do} = 0.1, q_{Dg} = 0.1$ and injection wells ($q_{Dw} = 1$). Capillary pressure is neglected (both N_b^{wo} and N_b^{og} are infinite).

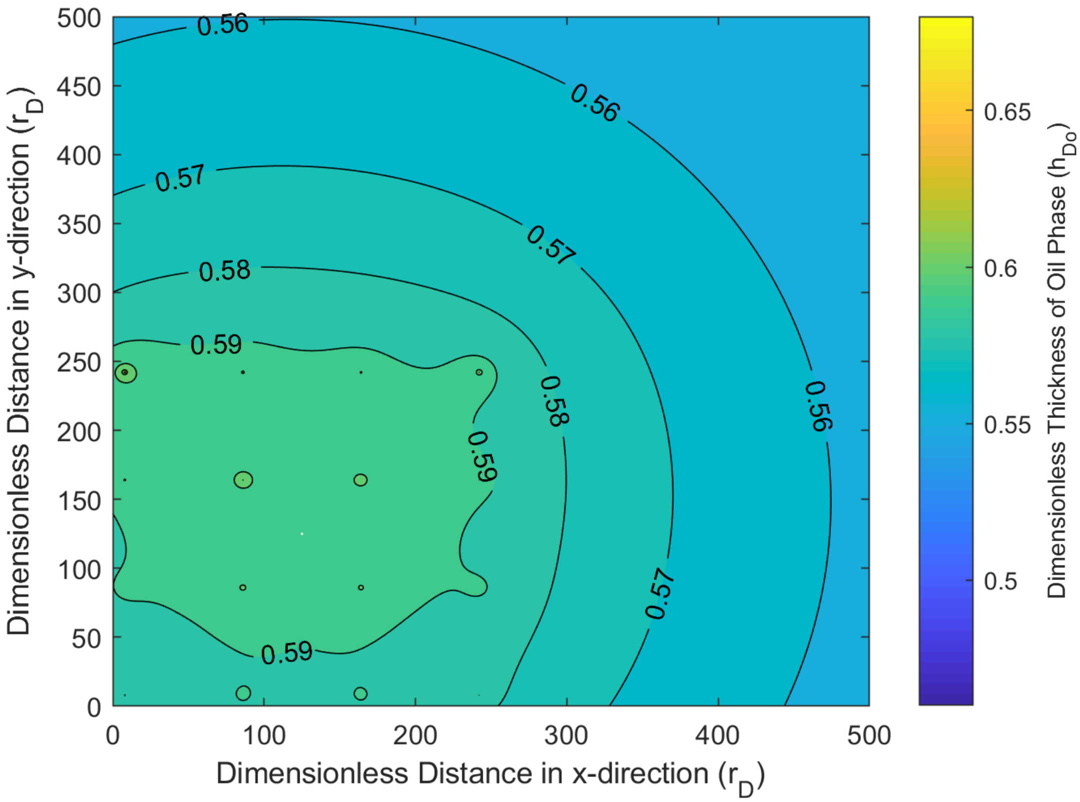

Figure 5.29 Contour map of the dimensionless oil phase thickness for an inverted five-spot pattern as shown in Figure 5.25. Figure 5.29 shows the case with production wells at $q_{Dw} = 0.5, q_{Do} = 0.4, q_{Dg} = 0.1$ and injection wells ($q_{Dw} = 1$). Capillary pressure is neglected (both N_b^{wo} and N_b^{og} are infinite).

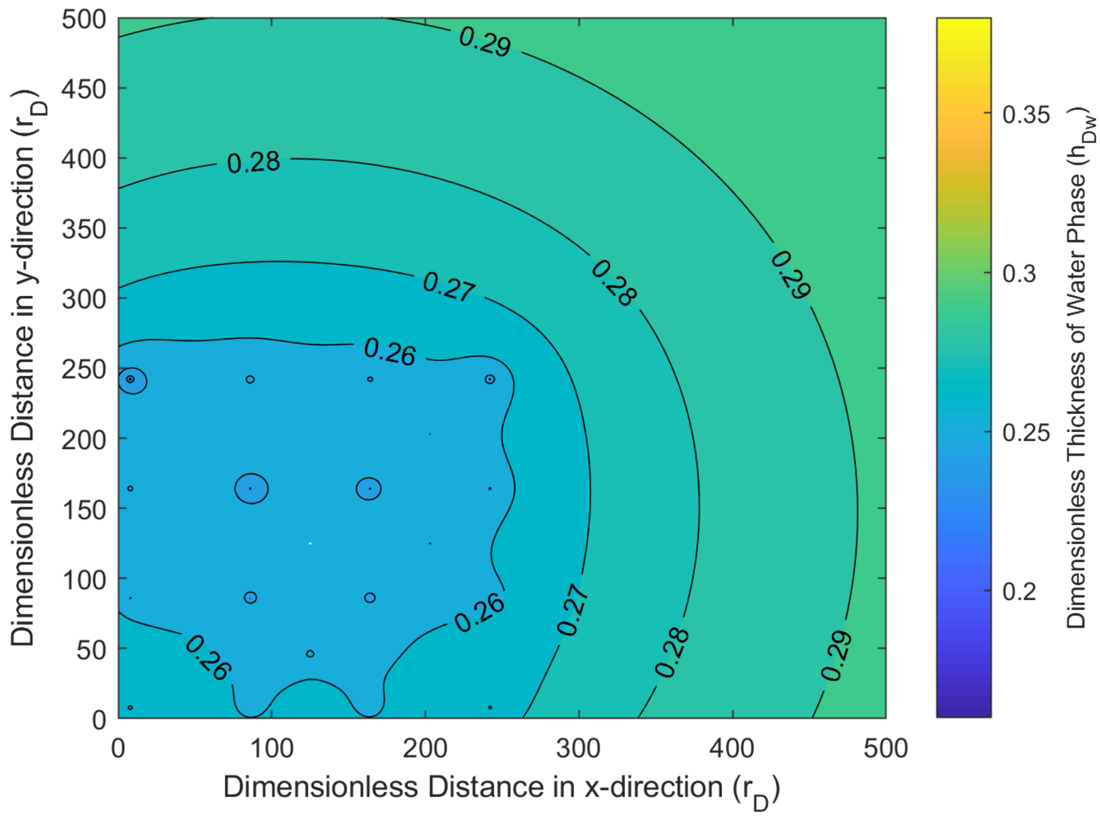

Figure 5.30 Contour map of the dimensionless water phase thickness for an inverted five-spot pattern as shown in Figure 5.25. Figure 5.30 shows the case with production wells at $q_{Dw} = 0.5, q_{Do} = 0.4, q_{Dg} = 0.1$ and injection wells ($q_{Dw} = 1$). Capillary pressure is neglected (both N_b^{wo} and N_b^{og} are infinite).

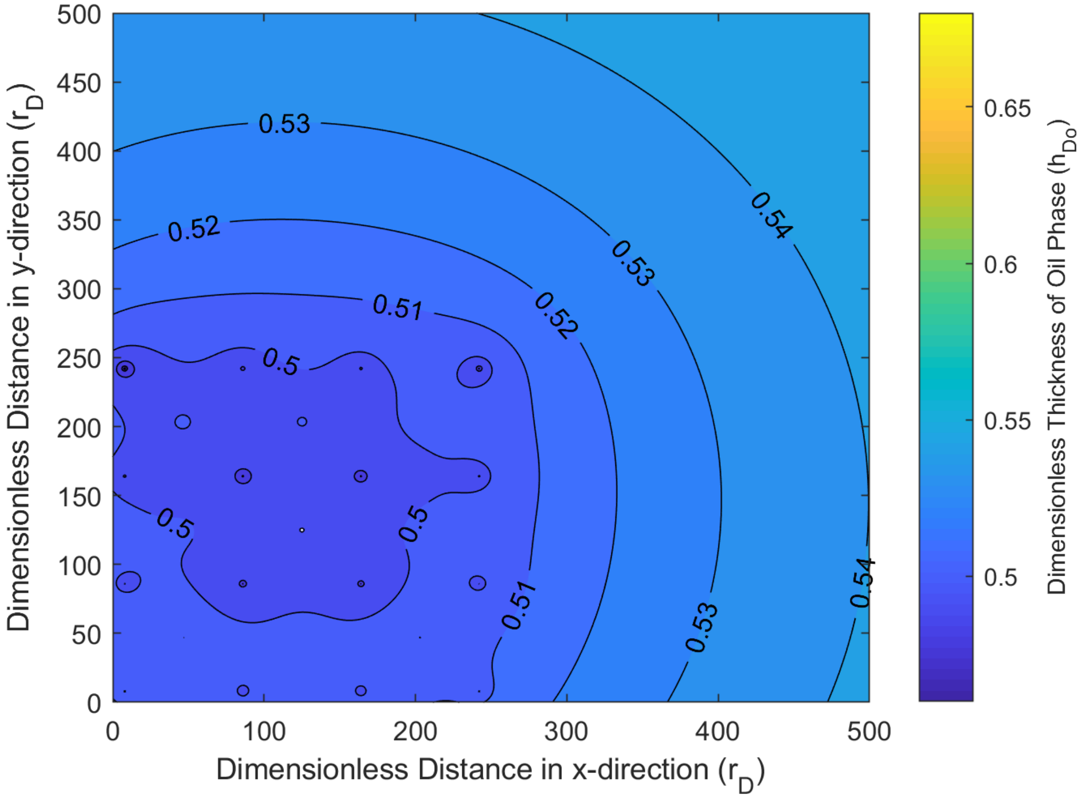

Figure 5.31 Contour map of the dimensionless oil phase thickness for an inverted five-spot pattern as shown in Figure 5.25. Figure 5.31 shows the case with production wells at $q_{Dw} = 0.2, q_{Do} = 0.7, q_{Dg} = 0.1$ and injection wells ($q_{Dw} = 1$). Capillary pressure is neglected (both N_b^{wo} and N_b^{og} are infinite).

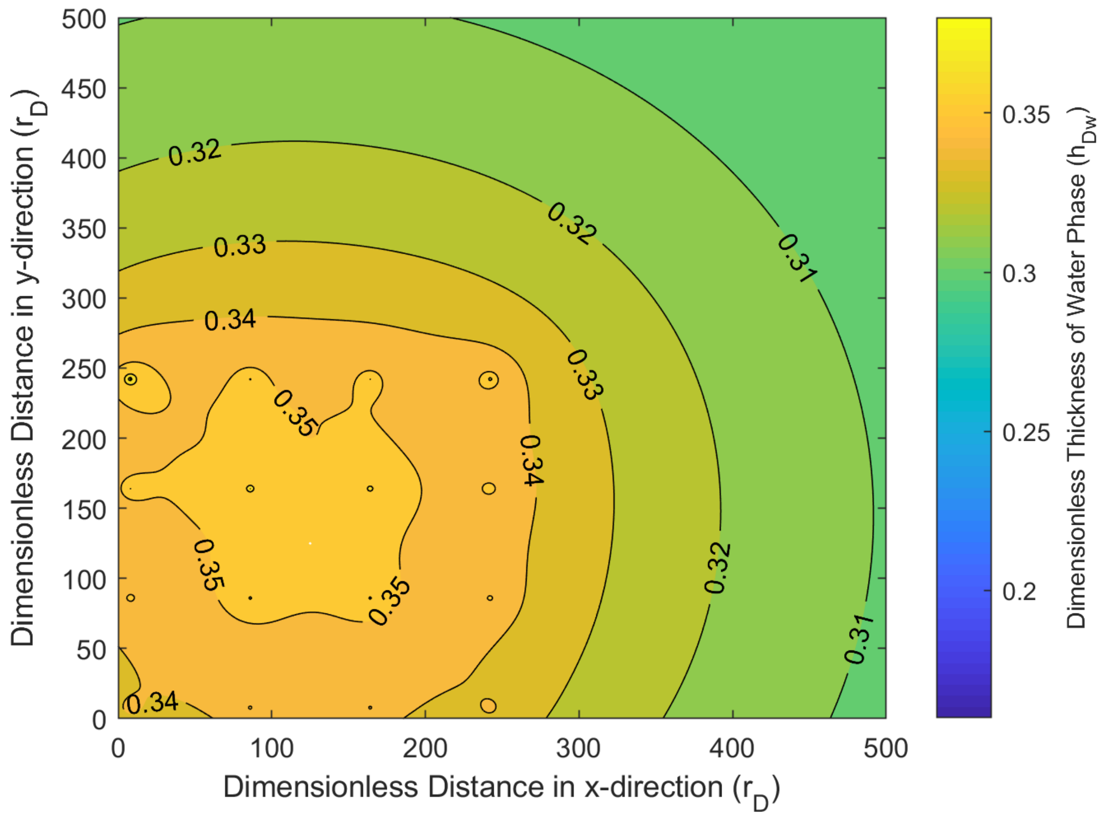

Figure 5.32 Contour map of the dimensionless water phase thickness for an inverted five-spot pattern as shown in Figure 5.25. Figure 5.32 shows the case with production wells at $q_{Dw} = 0.2, q_{Do} = 0.7, q_{Dg} = 0.1$ and injection wells ($q_{Dw} = 1$). Capillary pressure is neglected (both N_b^{wo} and N_b^{og} are infinite).

Chapter 6

CONCLUSIONS

6.1 Summary and Conclusions

Significant error exists near-wellbore in reservoir simulation due to coarsely-gridded blocks and error of Peaceman's well model. Many analytical solutions have been developed in the past and recently there have been several notable papers that have presented analytical coning solutions in a dimensionless "Dupuit form." Succeeding their work, we developed an analytical coning solution for simultaneous three-phase flow with and without capillary pressure for any number of vertical wells completed over the entire thickness of the reservoir. The solution assumes VE and steady-state flow and therefore gives the maximum crossflow and the greatest level of coning. The solution also allows for multiple wells using superposition and can be coupled to any relative permeability and capillary pressure model, although we used Stone 2 and Brooks-Corey here. The new solution is rapid and serves as a benchmark for numerical simulation. The following key conclusions are made:

- The new solution shows the sensitivity of the various phase thicknesses to individual flow rates. The critical oil rate can be increased by changing the water and gas flow rates.
- Inclusion of capillary pressure affects both gas and water coning. That is, the critical oil rate significantly decreases when capillary pressure is present.

- A new type of dimensionless IPW is generated where the total flow rate is kept constant. IPWs can be easily generated to demonstrate the change in the allowable physical rates, where the critical oil rate is a function of the flow rates of the other two phases.
- Multiple well cases were demonstrated using the principle of superposition, as is typically done in many analytical solutions. No-flow boundaries greatly affect the critical flow rate of the wells.

The limitations of the solution are that flow is steady-state and VE is assumed. The new solution could potentially be incorporated into Peaceman's well model to improve numerical prediction of coning. This could be done by generating the analytical solution within a grid block near the well.

6.2 Future Research

Based on the thesis, the possible research topics that could be conducted in the future are:

- The perforations are not explicitly specified in this thesis, in that the flow rates are assumed as shown. That is, we gave the coning levels for all possible combination of rates, so that in some cases these rates would require unusual perforation intervals to be achieved in practice. The perforation interval could be specified first and then flow rates determined in an iterative process by integration of Darcy's law for each phase over the perforated interval.

- This thesis only focused on coning behavior for vertical wells. The solution can be extended into a coning solution for horizontal wells. The basic idea is introduced in Phaiboonpalayoi and Johns (2016).
- As discussed, significant errors near-wellbore exists with the use of Peaceman's well model. Thus, the new solution could potentially be incorporated into Peaceman's well model to improve the numerical prediction of a coning behavior. This could be done by generating the analytical solution within a grid block near the well. This will be helpful in precisely describing the coning behavior near the wellbore region.
- The solution only includes drainage for relative permeability. However, it would be much more precise if both drainage and imbibition could be incorporated into the model.

REFERENCES

Abass, H. H., and Bass, D. M. (1988). The Critical Production Rate in Water-Coning System. SPE. https://doi.org/10.2118/17311-MS

Ansari, R. Z. (2006). *Superposition of Analytical Coning Solutions*. MS thesis. The University of Texas at Austin.

Ansari, R. Z., and Johns, R. T. (2013). Superposition of Steady-State Coning Solutions for Multiple Wells with Reservoir Boundaries. *Journal of Petroleum Science and Engineering*, *108*, 362–369. https://doi.org/10.1016/j.petrol.2013.07. 006

Armenta, M., and Wojtanowicz, A. (2002). Severity of Water Coning in Gas Wells. SPE. https://doi.org/10.2118/75720-MS

Arthur, M. G. (1944). Fingering and Coning of Water and Gas in Homogeneous Oil Sand. *Transactions of the AIME*, *155*(1), 184–201. https://doi.org/10.2118/944184-G

Brooks, R. H., and Corey, A. T. (1964). Hydraulic Properties of Porous Media. Colorado State University, Hydraulic Papers (3).

Chaney, P. E., Noble, M. D., Henson W. L., and Rice T. D. (1956). How to Perforate Your Well to Prevent Water and Gas Coning. *Oil & Gas Journal*, *55*(53), 108–114.

Chaperon, I. (1986). Theoretical Study of Coning Toward Horizontal and Vertical Wells in Anisotropic Formations: Subcritical and Critical Rates. https://doi.org/10. 2118/15377-MS

Chappelear, J. E., and Hirasaki, G. J. (1976). A Model of Oil-Water Coning for Two-Dimensional, Areal Reservoir Simulation. *SPE J*, *16*(2), 65–72. https://doi.org/ 10.2118/4980-PA

Charbeneau, R. J., Johns, R. T., Lake, L. W., and McAdams III, M. J. (2000). Free-Product Recovery of Petroleum Hydrocarbon Liquids. *Groundwater Monitoring & Remediation*, *20*(3), 147–158. https://doi.org/10.1111/j.1745-6592.2000.tb00280.x

Charbeneau, R. J., and Chiang, C. Y. (1995). Estimation of Free-Hydrocarbon Recovery from Dual-Pump Systems. *Groundwater*, *33*(4), 627–634. https://doi.org/10.1111/ j.1745-6584.1995.tb00318.x

Chierici, G. L., Ciucci, G. M., and Pizzi, G. (1964). A Systematic Study of Gas and Water Coning By Potentiometric Models. *Journal of Petroleum Technology*, *16*(8), 923–929. https://doi.org/10.2118/871-PA

Coats, K., Dempsey, J., and Henderson, J. (1971). The Use of Vertical Equilibrium in Two-Dimensional Simulation of Three-Dimensional Reservoir Performance. *Soc. Pet. Eng. J., Mar*, *251*, 63–71. https://doi.org/10.2118/2797-PA

Coats, K. H., Nielsen, R. L., Terhune, M. H., and Weber, A. G. (1967). Simulation of Three-Dimensional, Two-Phase Flow In Oil and Gas Reservoirs. *SPE J*, *7*(4). https://doi.org/10.2118/1961-PA

David, I., and Anim-Addo, S. B. (2004). Analytical Solutions for NAPL Recovery Using Complex Multiple Well Systems. *Developments in Water Science*, *55*(1), 449–460. https://doi.org/10.1016/S0167-5648(04)80072-8

Delliste, A. M. (1998). *Steady-State Coning Solutions for Multiphase Flow to a Well*. MS thesis. The University of Texas at Austin.

Dupuit, J. É. J. (1863). Études Théoriques et Pratiques sur le Mouvement des Eaux dans les Canaux Découverts et à Travers les Terrains Perméables, 2nd edition Dunod, Paris.

ECLIPSE. (2014). Schlumberger. Retrieved from https://www.software.slb.com /products/eclipse

Gunning, J., Paterson, L., and Poliak, B. (1999). Coning in Dual Completed Systems. *Journal of Petroleum Science and Engineering*, *23*(1), 27–39. https://doi.org/10.1016 /S0920-4105(99)00006-6

Guo, B., and Lee, R. L.-H. (1993). A Simple Approach to Optimization of Completion Interval in Oil/Water Coning Systems. *SPE Reservoir Engineering*, *8*(4), 249–255. https://doi.org/10.2118/23994-PA

Høyland, L. A., Papatzacos, P., and Skjaeveland, S. M. (1989). Critical Rate for Water Coning: Correlation and Analytical Solution. *SPE Reservoir Engineering*, *4*(4), 495–502. https://doi.org/10.2118/15855-PA

IMEX. (2017). Computer Modelling Group Ltd. Retrieved from https://www.cmgl.ca /imex

Jacks, H., Smith, O., and Mattex, C. (1973). The Modeling of a Three-Dimensional Reservoir with a Two-Dimensional Reservoir Simulator-The Use of Dynamic Pseudo Functions. *Old SPE Journal*.

Johns, R. T., Lake, L. W., Ansari, R. Z., and Delliste, A. M. (2005). Prediction of Capillary Fluid Interfaces During Gas or Water Coning in Vertical Wells. *SPE Journal*, (December). https://doi.org/10.2523/77772-MS

Kidder, R. E. (1956). Flow of Immiscible Fluids in Porous Media: Exact Solution of a Free Boundary Problem. *Journal of Applied Physics*, *27*, 867–869. https://doi.org/10.1063 /1.1722505

Killough, J. E., and Foster Jr., H. P. (1979). Reservoir Simulation of the Empire Abo Field: The Use of Pseudos in a Multilayered System. *Society of Petroleum Engineers Journal*, *19*(5). https://doi.org/10.2118/7418-PA

Lake, L. W., Johns, R. T., Rossen, W. R., and Pope, G. A. (2014). *Fundamentals of Enhanced Oil Recovery*.

Leeftink, T. N., Latooij, C. A., and Rossen, W. R. (2015). Injectivity Errors in Simulation of Foam EOR. *Journal of Petroleum Science and Engineering*, *126*, 26–34. https://doi.org/10.1016/j.petrol.2015.3.026

Martin, J. C. (1968). Partial Integration of Equations of Multiphase Flow. *SPE J*, *8*(4), 370–380. https://doi.org/10.2118/2040-PA

Meyer, H. I., and Garder, A. O. (1954). Mechanics of Two Immiscible Fluids in Porous Media. *Journal of Applied Physics*, *25*, 1954. https://doi.org/10.1063/1.1721576

Muskat, M., and Wycokoff, R. D. (1935). An Approximate Theory of Water-Coning in Oil Production. *Transactions of the AIME*, *114*(1), 144–163. https://doi.org/10.2118/935144-G

Obigbesan, A. B., Johns, R. T., Lake L. W., Bermudez, L., Hassan, M. R., Charbeneau, R. J. (2001). Analytical Solutions for Free-Hydrocarbon Recovery Using Skimmer and Dual-Pump Wells. SPE. https://doi.org/10.2118/66756-MS

Peaceman, D. W. (1978). Interpretation of Well-Block Pressures in Numerical Reservoir Simulation. *SPE J*, *18*(3), 183–194. https://doi.org/10.2118/6893-PA

Peaceman, D. W. (1983). Interpretation of Well-Block Pressures in Numerical Reservoir Simulation With Nonsquare Grid Blocks and Anisotropic Permeability. *SPE J*, *23*(3), 531–543. https://doi.org/10.2118/10528-PA

Phaiboonpalayoi, C., and Johns, R. T. (2016). Solution to Coning Under Simultaneous Three-Phase Flows for Multiple Vertical Wells. In *International Petroleum Technology Conference*. https://doi.org/10.2523/IPTC-18815-MS

Pietraru, V., and Le Bars, P. (1996). About Kinds of Breakthrough and Maximum Recovery Factor in Dual Coning. SPE. https://doi.org/10.2118/37049-MS

Piper, L. D., and Gonzalez Jr., F. M. (1987). Calculation of the Critical Oil Production Rate and Optimum Completion Interval (pp. 235–242). https://doi.org/10.2118/16206-MS

Pirson, S. J. (1977). *Oil Reservoir Engineering*. R. E. Krieger Pub. Co.

Sharma, A., Delshad, M., Huh, C., and Pope, G. (2011). A Practical Method to Calculate Polymer Viscosity Accurately in Numerical Reservoir Simulators. *Proceedings of SPE Annual Technical Conference and Exhibition*. https://doi.org/10.2118/147239-MS

Sharpe, H. N., and Ramesh, B. A. (1992). Development and Validation of a Modified Well Model Equation for Nonuniform Grids With Application to Horizontal Well and Coning Problems.

Shirman, E. I., and Wojtanowicz, A. K. (2000). More Oil Using Downhole Water-Sink Technology: A Feasibility Study. *SPE Production & Facilities*, *15*(4), 234–240. https://doi.org/10.2118/66532-PA

Shook, M., Li, D., and Lake, L. W. (1992). Scaling Immiscible Flow Through Permeable Media by Inspectional Analysis. *In Situ*, *16*(4), 311–349.

Siemek, J., and Stopa, J. (2002). A Simplified Semi-Analytical Model for Water-Coning Control in Oil Wells With Dual Completions System. *J. Energy Resour. Technol*, *124*(4), 246–252. https://doi.org/10.1115/1.1506699

Siripatrachai, N. (2016). Development of a Multi-Mechanistic Triple-Porosity, Triple-Permeability Compositional Model for Unconventional Reservoirs, (August).

Stone, H. L. (1973). Estimation of Three-Phase Relative Permeability And Residual Oil Data. *Journal of Canadian Petroleum Technology*, *12*(4), 53–61. https://doi.org/10.2118/73-04-06

Strack, O. D. L. (1989). *Groundwater Mechanics*. Prentice Hall.

Swisher, M. D., and Wojtanowicz, A. K. (1995). New Dual Completion Method Eliminates Bottom Water Coning. https://doi.org/10.1017/CBO9781107415324.004

Swisher, M. D., and Wojtanowicz, A. K. (1996). In Situ-Segregated Production of Oil and Water - A Production Method With Environmental Merit: Field Application. *SPE Advanced Technology Series*, *4*(2), 51–58. https://doi.org/10.2118/29693-PA

Tabatabaei, M., Ghalambor, A., and Guo, B. (2012). An Analytical Solution for Water Coning in Vertical Wells. *SPE Production & Operations*, *27*(2), 195–204. https://doi.org/10.2118/113106-PA

Utama, F. A. (2008). An Analytical Model to Predict Segregated Flow in the Downhole Water Sink Completion and Anisotropic Reservoir. SPE. https://doi.org/10.2118/120196-STU

Wheatley, M. J. (1985). An Approximate Theory of Oil/Water Coning. https://doi.org/10.2118/14210-MS

Yortsos, Y. C. (1995). A Theoretical Analysis of Vertical Flow Equilibrium. *Transport in Porous Media*, *18*(2), 107–129. https://doi.org/10.1007/BF01064674

Zapata, V. J., and Lake, L. W. (1981). A Theoretical Analysis of Viscous Crossflow. SPE. https://doi.org/10.2118/10111-MS

Appendix A

FLOW POTENTIAL

Flow potential for phase j is defined as,

$$\varphi_j = (p_j - p_{ref}) + \rho_j g(z - z_{ref}), \tag{A-1}$$

where, the reference pressure and elevation are arbitrary, but are fixed once defined. In this paper, we set the reference point at the bottom of the reservoir. The flow potentials for oil and gas phase are then given as:

$$\varphi_o = \varphi_w - \Delta\rho_{wo} g h_w, \tag{A-2}$$

$$\varphi_g = \varphi_o - \Delta\rho_{og} g(h_o + h_w), \tag{A-3}$$

where, $\Delta\rho_{wo} = \rho_w - \rho_o$ and $\Delta\rho_{og} = \rho_o - \rho_g$. Differentiation of Eqs. (A-2) and (A-3) with radial distance r gives,

$$\frac{d\varphi_w}{dr} - \frac{d\varphi_o}{dr} = \Delta\rho_{wo} g \frac{dh_w}{dr}, \tag{A-4}$$

$$\frac{d\varphi_o}{dr} - \frac{d\varphi_g}{dr} = \Delta\rho_{og} g \left(\frac{dh_o}{dr} + \frac{dh_w}{dr}\right). \tag{A-5}$$

Rearrangement of Eq. (A-4) gives:

$$\frac{dh_w}{dr} = \frac{1}{\Delta\rho_{wo}g}\left(\frac{d\varphi_w}{dr} - \frac{d\varphi_o}{dr}\right). \qquad \text{(A-6)}$$

Subtraction of Eq. (A-6) from Eq. (A-5) yields:

$$\frac{dh_o}{dr} = \left(\frac{1}{\Delta\rho_{og}g} + \frac{1}{\Delta\rho_{wo}g}\right)\frac{d\varphi_o}{dr} - \frac{1}{\Delta\rho_{og}g}\frac{d\varphi_g}{dr} - \frac{1}{\Delta\rho_{wo}g}\frac{d\varphi_w}{dr}. \qquad \text{(A-7)}$$

Since the thickness of the reservoir is constant ($h = h_w + h_o + h_g$), differentiation gives:

$$\frac{dh_w}{dr} + \frac{dh_o}{dr} + \frac{dh_g}{dr} = 0. \qquad \text{(A-8)}$$

Thus, from Eqs. (A-6) to (A-8):

$$\frac{dh_g}{dr} = \frac{1}{\Delta\rho_{og}g}\left(\frac{d\varphi_g}{dr} - \frac{d\varphi_o}{dr}\right). \qquad \text{(A-9)}$$

The volumetric flow rate of phase j at any radial location is:

$$q_j = 2\pi r \int_0^h u_j\, dz = 2\pi r \int_0^h \lambda_j \frac{d\varphi_j}{dr}\, dz, \qquad \text{(A-10)}$$

where, $u_j = -\lambda_j \frac{d\varphi_j}{dr}$. Under VE, the flow potential is only a function of r, hence, the radial derivative of the flow potential passes through the integral. Thus,

$$\frac{d\varphi_j}{dr} = -\frac{q_j}{2\pi r T_j}. \tag{A-11}$$

Substitution of Eq. (A-11) into Eqs. (A-6), (A-7) and (A-9), respectively, yields:

$$\frac{dh_w}{dr} = \frac{1}{\Delta\rho_{wo} g}\left(\frac{q_o}{2\pi r T_o} - \frac{q_w}{2\pi r T_w}\right), \tag{A-12}$$

$$\frac{dh_o}{dr} = \left(\frac{1}{\Delta\rho_{og} g}\right)\frac{q_g}{2\pi r T_g} + \left(\frac{1}{\Delta\rho_{wo} g}\right)\frac{q_w}{2\pi r T_w} - \left(\frac{1}{\Delta\rho_{og} g} + \frac{1}{\Delta\rho_{wo} g}\right)\frac{q_o}{2\pi r T_o}, \tag{A-13}$$

$$\frac{dh_g}{dr} = \frac{1}{\Delta\rho_{og} g}\left(\frac{q_o}{2\pi r T_o} - \frac{q_g}{2\pi r T_g}\right). \tag{A-14}$$

Eqs. (A-12) to (A-14), respectively, give the thickness of the water, oil and gas phase as a function of r.

Appendix B

AVERAGED RELATIVE PERMEABILITY

In the solutions, the average relative permeability at a fixed location over the entire thickness of the reservoir must be calculated (see Eq. (2)). In this paper, we followed the same steps as previous studies have done (Delliste, 1998; Johns et al., 2005; Ansari, 2006; Ansari and Johns, 2013; Phaiboonpalayoi and Johns, 2016). The vertically averaged relative permeability in a dimensionless form is defined as,

$$\bar{k}_{rj} = \int_0^1 k_{rj}\, dz_D. \qquad \text{(B-1)}$$

The averaged relative permeability for each phase is affected by the vertical saturation distribution (these are pseudo-relative permeabilities for coning). We have used Stone 2 model as a relative permeability although any model can be used in the solution. For relative permeability for each phase, we have implemented Newton-Cotes formula (11-point closed rule).

For Stone 2 model (1973), the relative permeability for each phase is given by,

$$k_{rw} = k_{rw}^{\circ}\left(\frac{S_w - S_{wr}}{1 - S_{wr} - S_{or}^{wo}}\right)^{n_1}, \qquad \text{(B-2)}$$

$$k_{ro} = k_{ro}^{\circ}\left\{\left(\frac{k_{row}}{k_{ro}^{\circ}} + k_{rw}\right)\left(\frac{k_{rog}}{k_{ro}^{\circ}} + k_{rg}\right) - k_{rw} - k_{rg}\right\}, \tag{B-3}$$

$$k_{rg} = k_{rg}^{\circ}\left(\frac{1 - S_w - S_o - S_{gr}}{1 - S_{wr} - S_{gr}}\right)^{n_3}. \tag{B-4}$$

where,

$$k_{row} = k_{ro}^{\circ}\left(\frac{1 - S_w - S_o - S_{or}^{wo}}{1 - S_{wr} - S_{or}^{wo}}\right)^{n_{21}}, \tag{B-5}$$

$$k_{rog} = k_{ro}^{\circ}\left(\frac{S_o + S_w - S_{or}^{og} - S_{wr}}{1 - S_{gr} - S_{or}^{og} - S_{wr}}\right)^{n_{23}}. \tag{B-6}$$

Stone 2 assumes the water phase is wetting, while gas is non-wetting and oil is the intermediate wetting phase. The corresponding Brooks-Corey capillary pressure model (1964) with the same wetting assumption is:

$$p_c = p_d S^{-1/n}, \tag{B-7}$$

where, S is the normalized saturation of phase j.

The integration in Eq. (B-1) must be done piece-by-piece depending on the value of capillary pressure. For example, above the oil-gas entry pressure, the wetting phase saturation is the liquid phase saturation where,

$$S_l = S_w + S_o = S_{lr} + (1 - S_{lr})\left(\frac{p_c^{og}}{p_d^{og}}\right)^{-\lambda}, \tag{B-8}$$

and $S_{lr} = S_{wr} + S_{or}^{og}$. When N_b^{wo} and N_b^{og} are infinite (capillary pressure is neglected), vertically averaged relative permeability of each phase from integration gives,

$$\bar{k}_{rw} = h_{Dw}, \tag{B-9}$$

$$\bar{k}_{ro} = h_{Do}, \tag{B-10}$$

$$\bar{k}_{rg} = h_{Dg}. \tag{B-11}$$

More details can be found in Phaiboonpalayoi and Johns (2016).